Journal Pre-proof

Sparsely PEGylated poly(beta-amino ester) polyplexes enhance antigen specific T-cell response of a bivalent SARS-CoV-2 DNA vaccine

Hulya Bayraktutan, Peter Symonds, Victoria A. Brentville, Cara Moloney, Charlotte Galley, Clare L. Bennett, Alvaro Mata, Lindy Durrant, Cameron Alexander, Pratik Gurnani

PII: S0142-9612(24)00181-9

DOI: https://doi.org/10.1016/j.biomaterials.2024.122647

Reference: JBMT 122647

To appear in: *Biomaterials*

Received Date: 8 January 2024

Revised Date: 29 May 2024

Accepted Date: 30 May 2024

Please cite this article as: Bayraktutan H, Symonds P, Brentville VA, Moloney C, Galley C, Bennett CL, Mata A, Durrant L, Alexander C, Gurnani P, Sparsely PEGylated poly(beta-amino ester) polyplexes enhance antigen specific T-cell response of a bivalent SARS-CoV-2 DNA vaccine, *Biomaterials*, https://doi.org/10.1016/j.biomaterials.2024.122647.

Sparsely PEGylated poly(beta-amino ester) polyplexes enhance antigen specific T-cell response of a bivalent SARS-CoV-2 DNA vaccine

Hulya Bayraktutan,[a,b] Peter Symonds,[c] Victoria A Brentville,[c] Cara Moloney,[a,b] Charlotte Galley,[d] Clare L. Bennett,[d] Alvaro Mata,[e,f] Lindy Durrant,[c] Cameron Alexander [a*] and Pratik Gurnani [g*]

[a] Division of Molecular Therapeutics and Formulation, School of Pharmacy, University of Nottingham, Nottingham, NG7 2RD, UK

[b] Biodiscovery Institute, School of Medicine, University of Nottingham, Nottingham, NG7 2UH UK

[c] Scancell Ltd, University of Nottingham Biodiscovery Institute, Nottingham, NG7 2RD, UK

[d] Department of Haematology, UCL Cancer Institute, 72 Huntley Street, University College London, London, UK, WC1E 6DD.

[e] Division of Regenerative Medicine and Cellular Therapies, School of Pharmacy, University of Nottingham, NG7 2RD UK

[f] Department of Chemical and Environmental Engineering, University of Nottingham, Nottingham, NG7 2RD

[g] UCL School of Pharmacy, University College London, 29-39 Brunswick Square, London, WC1N 1AX, UK

Abstract

DNA technology has emerged as a promising route to accelerated manufacture of sequence agnostic vaccines. For activity, DNA vaccines must be protected and delivered to the correct antigen presenting cells. However, the physicochemical properties of the vector must be carefully tuned to enhance interaction with immune cells and generate sufficient immune response for disease protection. In this study, we have engineered a range of polymer-based nanocarriers based on the poly(beta-amino ester) (PBAE) polycation platform to investigate the role that surface poly(ethylene glycol) density has on pDNA encapsulation, formulation properties and gene transfectability both in vitro and in vivo. We achieved this by synthesising a non-PEGylated and PEGylated PBAE and produced formulations containing these PBAEs, and mixed polyplexes to tune surface PEG density. All polymers and co-formulations produced small polyplex nanoparticles with almost complete encapsulation of the cargo in all cases. Despite high gene transfection in HEK293T cells, only the fully PEGylated and mixed formulations displayed significantly higher expression of the reporter gene than the negative control in dendritic cells. Further in vivo studies with a bivalent SARS-CoV-2 pDNA vaccine revealed that only the mixed formulation led to strong antigen specific T-cell responses, however this did not translate into the presence of serum antibodies indicating the need for further studies into improving immunisation with polymer delivery systems.

Key words: vaccine, DNA, delivery, nanoparticle, poly(beta-amino) ester, polyplex, COVID-19, SARS-CoV-2

Introduction

Vaccines are a critical form of prophylactic medicine, which have prevented more deaths than any other medical intervention in history [1]. Despite this, there is still a need to enhance the safety profile, boost efficacy in poorly vaccine-responsive segments of the population and accelerate manufacturing in order to respond rapidly to epidemic and pandemic scenarios [2]. DNA vaccines offer many of these advantages [3]. They operate by administering antigen encoding DNA which instructs local cells at the injection site to express a pathogen related antigen, initiating immunisation and thus protection against disease when challenged by the pathogen itself [3] [4] [5]. Although mRNA vaccines have been popularised throughout the COVID-19 pandemic, the overall stability of DNA compared to mRNA may enable DNA technologies to be utilised more widely in low to middle income countries, where access to cold-chain storage is limited [6].

The poor cellular association of DNA when administered 'naked', necessitates the development of safe and effective delivery systems to transport the nucleic acid vaccine construct to dividing cells [7]. The majority of clinical studies for DNA vaccines and therapies have utilised physical delivery systems, such as electroporation [8], jet-injectors [9], or gene gun systems [10], for intradermal administration [9], which is exemplified with the only licensed plasmid DNA vaccine, ZyCoV-D (Cadilla Healthcare) for COVID-19 which was approved for emergency use in India [11]. However, the lack of scalability for this approach and advanced training requirements for healthcare professionals means that these delivery approaches may not be appropriate in rapid response indications. While adeno-associated virus (AAV) vectors overcome some of these challenges, packaging constraints, expensive cell-based manufacture and potentially harmful immunogenic responses necessitates the need for alternative vectors [12]. For this reason, significant efforts have been placed on developing non-viral nanoparticle-based delivery systems which offer unlimited cargo capacity, biologic free manufacture, and reduced safety concerns [13-15].

Cationic polymers have emerged as a highly versatile nucleic acid delivery platform, which operate by condensing negatively nucleic acids into small, 50-200 nm diameter, nanoparticles typically termed 'polyplexes', assembled through supramolecular electrostatic interactions [16, 17]. Such polyplex nanoparticles stabilise the nucleic acid cargo and facilitate transportation across the physiological and cellular barriers required [18]. Although lipid nanoparticles have been the most accepted delivery approach since their use in the two licensed mRNA COVID-19 vaccines [19-21], polycations offer a significantly broader chemical space to tune formulation stability [22] and specificity towards immune cells, which are vital for vaccination. However, the high charge density on the polyplex surface means that there are potential toxicity concerns arising from cell membrane disruption, non-specific protein absorption, pain at the injection site or generalised reactogenicity towards the vaccine. To date, most researchers have focused on tuning the polymer composition and architecture to circumvent these outstanding challenges [23, 24].

One especially popular strategy has been to attach poly(ethyleneglycol) (PEG) chains to the surface of polyplexes to attenuate their interaction with the cell membrane [25]. However, there is limited understanding on how PEG grafting density may influence expression and tolerability of a DNA vaccine. This is particularly important in a vaccine setting where the formulation itself may

play a substantial role in activating specific cellular immunity pathways through membrane damage as has been seen with the LNPs for the two licensed COVID-19 vaccines. [26-28]

In this study we explore the relationship between PEG density on the surface of polyplexes and their ability to deliver plasmid DNA in vaccine-relevant *in vitro* and *in vivo* models. For this we prepared PEGylated and non-PEGylated poly(beta-amino) esters (PBAEs) as hydrolytically degradable, non-toxic, and efficient nucleic acid binding polycations. We demonstrated the high tolerability, potent transfection efficiency and fast intracellular trafficking of pDNA loaded polyplexes derived from each of these materials in HEK293T cells and a dendritic cell line. PEG density was modulated by preparing polyplexes containing mixtures of the polycations. The library of polycations was then further examined *in vivo* for their performance as delivery vectors for pDNA vaccines by formulating them with a bivalent SARS-CoV-2 vaccine encoding for the spike and nucleocapsid proteins, with the mixed polycation formulation eliciting strong antigen specific T-cell response (Figure 1).

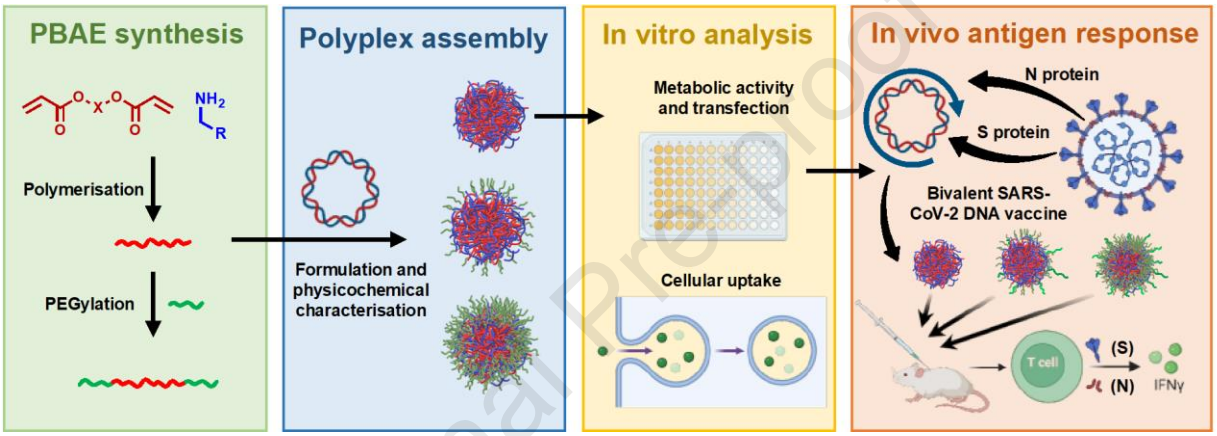

Figure 1. Schematic representation of PBAE synthesis, polyplex assembly, in vitro analysis and in vivo antigen response of a bivalent SARS-Cov-2 pDNA vaccine.

Materials and Methods

Materials

1,4-butanediol diacrylate (BDD), 5-aminopentan-1-ol (5-AP), triethylamine (TEA), PEG-thiol (mPEG-SH), Fluorescein isothiocyanate (FITC), diethyl ether, tetrahydrofuran, sodium acetate (NaOAc) buffer (pH:5.0), HEPES (4-(2-hydroxyethyl)-1-piperazineethanesulfonic acid), tannic acid, dye Gel Red, L-glutamine, Goat-anti-mouse IgG, Fc biotin and red CellMask™ Plasma Membrane stain were purchased from Sigma-Aldrich. Dimethyl sulfoxide (DMSO), loading buffer, Tris-acetate-EDTA (TAE) buffer, Lipofectamine 2000, 2-mercaptoethanol, Hoechst 33342, Lysotracker red and 96-well plates were obtained from ThermoFisher. Dulbecco's Modified Eagle Medium (DMEM) cell culture medium, RPMI 1640 cell culture medium, fetal bovine serum (FBS) and Opti-MEM were bought from Gibco, Invitrogen, Carlsbad, CA, USA. PrestoBlue reagent and ONE-Glo D-luciferin substrate were purchased from Promega, UK. Finally, S1 protein (Z03501) and N protein (Z034880) were obtained from GenScript.

Instrumentation and Analysis

NMR Spectroscopy

All ^{1}H-NMR spectra were recorded in ppm (δ) at 400 MHz in d6-DMSO using a Bruker Advance III MHz spectrometer that was maintained at 25°C. To analyse the spectra MestReNova 6.0.2 copyright 2009 (Mestrelab Research S.L.) was applied.

Gel permeation Chromatography
The gel permeation chromatography (GPC) analysis was performed using the PL-50 instrument equipped with a dual angle light scatter (LS), viscometry (VS) and differential refractive index (DRI) detection. The system was equipped with a PLgel 5 µm guard column and a 2 × PLgel Mixed D columns (300 × 7.5 mm). Dimethylformamide (DMF) with LiBr was utilised as an eluent with a flow rate of 1 mL/min at 50°C. The instrument was calibrated through Poly(methyl methacrylate) standards (Agilent EasyVials) between 550-955500 g mol^{-1}. Using conventional calibration, Cirrus GPC software, dispersity (*Đ*) values, molecular weight (M_w) and experimental molar mass ($M_{n,SEC}$) were detected.

Theoretical Molar Mass Calculation
The theoretical number average molar mass ($M_{n,th}$) was calculated as demonstrated in the following:

DLS and Zeta Potential
The dynamic light scattering (DLS), Zetasizer nano-ZS90 (Malvern, Inc.), instrument was used to characterise the particles in terms of the size, PDI and zeta potential. The instrument was used at 25°C to determine the zeta potential, average hydrodynamic diameters, and polydispersity index (PDI) of polyplexes.

Transmission Electron Microscopy
Briefly, glow discharged Formvar/carbon coated TEM grids were used, on which were placed the formulation samples (13 µL), which were left for 15 minutes, then the excess solution was removed, and the samples allowed to dry at room temperature. Following this, 10 µL of 2% aqueous uranyl acetate was applied to each grid and left for 10 seconds. After air drying, imaging was performed using a Tecnai G2 Spirit TEM with BioTwin lens configuration (Thermo Fisher Scientific, Eindhoven, The Netherlands) at an accelerating voltage of 100kV.

Polymer Synthesis and Characterisation

PBAE synthesis
PBAEs were synthesised using the following two-step general procedure. BDD and 5-AP were mixed at 1.1:1 (diacrylate:amine) molar ratio into a test tube (20 mL). The components were dissolved in DMSO to reach a concentration of 0.5 mg/mL, then a stir bar was added, and a rubber septum was used to seal the tube. The mixture was heated in the dark at 90°C for 24 h with continuous stirring at 300 rpm. The reaction mixture was then used directly for end-capping as detailed below.

End capping for non-PEGylated PBAEs
To produce non-PEGylated PBAEs, an excess amount of 5-amino-1-pentanol was added directly to the PBAE solution for 24 h at room temperature. Polymers were isolated by diluting the reaction mixture into 1-fold volume of tetrahydrofuran (e.g. 5 mL of DMSO and 5 mL of tetrahydrofuran) followed by dropwise precipitation in diethyl ether. The polymer was collected via centrifugation and dried under reduced pressure at 37°C to yield a yellow viscous liquid Finally, polymers were stored at -20°C as solutions (100 mg/mL) in DMSO.

End capping for PEGylated PBAEs
To obtain PEG-PBAE-PEG triblock copolymers, the initial non-endcapped PBAE solution was mixed with 800 Da methoxy-PEG-thiol (mPEG-SH) polymer at a molar ratio of 1:2.5

acrylate:mPEG-SH in DMSO containing TEA (0.1 molar equivalents relative to thiol) at room temperature for 24h. The PEGylated PBAE was isolated and stored as described above.

Synthesis of Fluorescently Labelled PBAEs
Fluorescently labelled PBAEs, OH-(pBDD-5AP)-OH and PEG-(pBDD-5AP)-PEG were synthesised using the following generation procedure. PBAEs were dissolved in 5 mL DMSO (0.5 mg/mL) in a 20 mL vial. FITC was added to vials at a 1:10 (moles of end amine: FITC) molar ratio and TEA was added to the mixture at a 0.1 molar ratio. The reaction mixture was allowed to stir for 24 h in the dark at room temperature. The reaction mixture was then dialysed using molecular weight cut-off 3,5 kDa against 250 mL NaOAc buffer (pH:5.0), in the dark. Purification was continued for 4 days and the dialysis medium refreshed 2 times in a day. After freeze drying, FITC-labelled polymers were collected as a yellow solid and were stored at -20°C as solutions (100 mg/mL) in DMSO.

Polymer Buffering Capacity Assay
The buffering capacity of PEGylated and non-PEGylated polymers was evaluated by acid-base titration over the pH range of 10.0–3.0. Briefly, 2 mg of polymer was dissolved in 30 mL of 0.1 M NaCl aqueous solution, and the solution was adjusted to pH 10.0 using 0.1 M NaOH. Then, precise volumes (between 10-20 uL) 0.1 M HCl were added until a pH of 3 was achieved. The pH after each addition of HCl was recorded. 0.1 M NaCl was set as negative control.

Synthesis of pDNA

Two different types of pDNA (luciferase and green fluorescent protein (GFP)) (Addgene #693601) was transformed into *Escherichia coli* and cultured in 100 mL of Luria broth (LB) with 100 µg/mL of ampicillin. The pDNA was isolated using a kit Plasmid Plus MidiPrep (QIAGEN, UK). The concentration and purity of pDNA was measured on a NanoDrop One (ThermoFisher, UK) and Agarose gel electrophoresis, respectively.

Preparation of Polyplexes

Polyplexes were prepared between positively charged polymers and negatively charged DNA by mixing various w/w ratios (32, 64 and 128). Firstly, the working dilutions of polymers and DNA were prepared in 25mM NaOAc buffer (pH:5.0). Depending on the desired w/w ratio, differing amounts of polymer stock solutions were mixed with nucleic acids in the buffer, gently mixed using a pipette and incubated at room temperature for 30 minutes. Whilst preparing the PBAE/DNA complexes, taking a w/w 64 ratio as an example, 10 µg/mL of the DNA stock solution was mixed with 2.560 mg/mL PBAE by pipette using a 25mM NaOAc buffer.

PEG-tannin binding assay

Tannic acid was diluted to a concentration of 10 µg mL^{-1} in pH 5 sodium acetate buffer. PEG-(pBDD-5AP)-PEG, OH-(pBDD-5AP)-OH and mixed nanoparticle suspensions were prepared as mentioned above at a w/w ratio 64. Subsequently, 1 mL of each nanoparticle suspension were transferred to a polystyrene cuvette and placed in an Agilent-Cary UV-VIS spectrometer. Absorbance readings at 500 nm were taken continuously at intervals of 1 millisecond (ms). After approximately 65 s, 0.3 mL of the tannic acid solution was added and mixed via micropipette. The absorption was then observed for a further 2 minutes.

Gel retardation assay

A 1% agarose gel was prepared in 50 mL TAE buffer (40mM Tris-acetate, 1mM EDTA) using a microwave (approximately 40 seconds) to dissolve the gel and then was stained with the 2 µL of dye Gel Red for the nucleic acid bands' visualization. Finally, 10 µL of nanoparticle solution were mixed with 2 µL of loading buffer, after pipette, 12 µL of the solutions were loaded in each well. Electrophoresis was conducted for 45 minutes at 90V. The visualisation of the DNA bands was detected with a UV detector (Bio-Rad) at 312nm.

In Vitro Experiments

Cell Culture
HEK293T cells were a gift from Imperial College London and cultured in 10 % (v/v) FBS containing high glucose DMEM cell culture medium. DC2.4 cells were obtained from ATCC and cultured in RPMI 1640 cell culture medium. Media containing L-glutamine was supplemented with 4-(2-hydroxyethyl)-1-piperazineethanesulfonic acid (10mM), non-essential amino acids (0.1mM) and 10 % FBS. Absence of mycoplasma was confirmed using polymerase chain reaction. Cells were grown to 90 % confluence in a humidified incubator at 37°C (5% CO2) and detached with 1x trypsin/EDTA. Viability was assessed using Trypan Blue staining.

Cell Viability Assays
To investigate the cytotoxicity of the formulations, a cell viability assay was performed using HEK293T and DC2.4 cell lines. 24 hours prior to treatment, cells were seeded in a clear 96-well plate at a density of $20x10^3$ cells/well. For the treatment, the medium was aspirated, and cells were treated with 200 µL of Opti-MEM containing various w/w ratios of formulations complexed with 10 µg/mL fluc pDNA concentration (20 µL of polyplex solution). After 4 hours, nanoparticle solutions were aspirated and 100 µL of complete medium was added to wells. At 24 hours posttreatment, each well was treated with 100 µL of 10% PrestoBlue reagent and allowed to incubate for 1 h. Then, the total volume was transferred to a black 96-well plate and the FLUOstar Omega plate reader (BMG LABTECH, UK) was used to determine the fluorescent intensity (540 nm – 590 nm) of each well and normalized to the medium control.

In Vitro Transfection Experiments
In vitro transfection experiments were performed using HEK293T and DC2.4 cell lines and commercially available transfectant agent Lipofectamine 2000 was used as positive control. 24 hours prior to treatment, cells were seeded in a clear 96-well plate at a density of $20x10^3$ cells per well. For the treatment, the medium was aspirated, then cells were transfected with 200 µL of Opti-MEM containing various w/w ratios of formulations complexed with 10 µg/mL fluc pDNA concentrations (20 µL of polyplex solution). After 4 hours, nanoparticle solutions were aspirated and 100 µL of medium was added to wells. At 24 hours posttreatment, 50 µL of media was removed then 50 µL of the ONE-Glo D-luciferin substrate was placed into each well and mixed well by pipette. Finally, the total 100 µL was placed in a 96-well plate and FLUOstar Omega plate reader (BMG LABTECH, UK) was used to determine the luminescence.

In Vitro Bone marrow dendritic cell (BM DC) Transfection Experiments
C57BL/6 female mice were purchased from Charlie River UK. *In vitro* procedures were conducted in accordance with the Ethics and Welfare Committee of the Comparative Biology Unit (UCL, London, UK) was carried out under a Home Office Project Licence (PP4506002). Femurs and tibias of 6-8 week old C57BL/6 female mice were collected and bone marrow cells were harvested by mortar and pestle in complete RPMI media. Red blood cells were lysed with ACK lysis buffer

and washed with complete media. Remaining progenitor cells were plated $1.5x10^6$ cells/ml in a 24 well non tissue culture treated plate with 20ng/ml GM-CSF. On day 2 of the culture, 800 µL of the existing media in each well was used to wash the well to detach lightly adhered cells. 800 µL of the media was then removed and replaced with 1 mL fresh media containing 20ng/ml GM-CSF. On day 5, 1 mL of media was removed from each well and replaced with 1 mL fresh media containing 20 ng/ml GM-CSF. On day 7, cells were detached using trypsin-EDTA and reseeded at a $0.5x10^6$ cells/mL in a 24 well non tissue culture treated plate. On day 8, BM DCs were transfected with the polyplexes at 5 µg/mL DNA and 320 µg/mL PBAE concentrations and left for 24 h incubation. On day 9 cells were harvested and labelled for surface staining CD11c, CD45, CD24, SIRPa, B220, XCR1, CD11b, CD86, Ly6c, MHC II and viability dye. Flow cytometer data was collected on a Fortessa instrument and analysed via FlowJo soiftware.

eGFP Expression of pDNA

To visualise transfection efficiency, GFP encoded pDNA + BDD-mPEG (w/w 64) formulation was prepared and eGFP expression was monitored. Briefly, HEK293T cells were plated in CellView™ 35 mm diameter glass bottom cell culture dishes at a density of $40x10^4$ cells per well 24 h prior to transfection. For the treatment, the medium was aspirated, and cells were transfected with Opti-MEM containing BDD-mPEG + pDNA (10 µg/mL). Cells were incubated for 4 hours at 37°C with 5% CO_2. Then, nanoparticles were aspirated, and cells washed 3 times with PBS and stained with 10 µg/mL Hoechst 33342 and 10 µg/mL red CellMask™ Plasma Membrane stain applied in PBS solution. After 30 minutes, the staining solution was aspirated, and cells were washed 3 times with PBS then FluoroBrite DMEM was added to cells. Imaging was performed using confocal microscopy (Leica, Germany) using LAS X software on DAPI and GFP filters. ImageJ software was used to analyse the microscopy data.

Cellular Uptake of pDNA using Confocal Microscopy

DC2.4 cells were seeded in CellView™ 35 mm diameter glass bottom cell culture dishes at a density of 30 x 10^4 cells per well. For the treatment, the medium was aspirated, and cells were transfected with Opti-MEM containing FITC labelled BDD-mPEG + pDNA (0.01 mg/mL). Cells were incubated for 1 and 4 hours at 37°C with 5% CO2. Then, nanoparticle solutions were aspirated, and cells washed 3 times with PBS and stained with 10 µg/mL Hoechst 33342 and 75nM Lysotracker red applied in PBS solution. After 30 minutes, the solution was aspirated again, and cells were washed 3 times with PBS then FluoroBrite DMEM was added to cells. Imaging was performed using Leica confocal microscopy with LAS X software on DAPI, FITC and Lysotracker filters. ImageJ software was used to process the images.

Imaging Cytometry

DC2.4 cells were seeded in a clear 6-well plate at a density of 40 x 10^5 cells per well. For the treatment, the medium was aspirated, and cells were transfected with Opti-MEM containing BDD-mPEG + pDNA (0.01 mg/mL) formulation. After 4 hours, the nanoparticle solutions were aspirated and 150 µL of 0.05% trypsin was used for detachment of cells from wells. After incubation for 15 minutes, 300 µL FACS buffer was used to neutralise the trypsin and cells were centrifuged at 1500 rpm for 10 minutes. Following this, cells were stained with Zombie Violet (1:500) dye for 30 minutes at room temperature to help with gating on live cells. Then, cells were fixed with 100 µL of 4% paraformaldehyde in PBS for 20 minutes. Fixed cells were centrifuged, and pellets resuspended in 50 µL of PBS. Data were acquired using an Image Stream 100 (Amnis, Seattle, US) and on single cell in focus circumstances was used for analysis. Ideas Software (Amnis, Seattle, WA, USA) was used for data analysis. Total cell fluorescence was calculated by default

total cell masks for the measurement of the nanoparticle internalisation and cell interiors were identified using the area erode tool (brightfield channel). Internalisation index was shown as percentage of maximum internalisation (percentage of interior cell fluorescence to total cell fluorescence).

In Vivo Experiments

Mice and Immunisations

Animal work was carried out under a Home Office Project Licence (PP2706800). Mice were maintained in the animal unit at Nottingham Trent University according to Home Office guidelines and the Project Licence. Studies were approved by both University of Nottingham and NTU AWERBs (animal welfare and ethical review boards). There were 4 different groups and each group contained three female Balb/C (Charles River) mice aged 8-12 weeks. All mice in the positive control group received DNA (SN17, which was gifted by Scancell Ltd., Nottingham, UK) coated onto 1.0 µm gold particles (BioRad, Hemel Hempstead, UK) and applied intradermally to the mice via gene gun (BioRad, UK) on days 1, 8 and 15 [29]. Mice in other three groups received a single 50 µL injection of nanoparticle solution containing 5 µg SN17 with PBAE-PEG-based polymers (BDD, mPEG-BDD and Mix). First, nanoparticles were prepared at concentrations of 40 µg/mL and then were centrifuged using Amicon® Ultra-15 Centrifugal Filter Unit to obtain the above-mentioned desired concentrations. Then, concentrated nanoparticle solutions were applied as intramuscular (im) injection on days 1,8 and 15. On day 21 mice were sacrificed.

IFN-γ ELISpot Assay

Splenocytes harvested from mice from each group were treated and assayed independently. Ex vivo ELISpot assays were used to detect T cell responses using murine IFNγ capture and detection reagents, S1 and N proteins (SinoBiological and Genscript respectively), according to the manufacturer's instructions (Mabtech AB, Nacka Strand, Sweden). In brief, capture antibodies were coated onto wells of 96-well Immobilin-P plate and triplicate wells were seeded with $5x10^5$ splenocytes in complete media (RPMI medium 1640) supplemented with 10% FCS, 2mM L-glutamine and sodium bicarbonate buffered with additional 20mM HEPES containing 50µM 2-mercaptoethanol. Synthetic peptides (as detailed above) were used at a final concentration of 5 µg/mL in complete media plus 2-mercaptoethanol and added to these wells. Whole proteins were used at a final concentration of 1µg/mL. Following incubation, captured antibody was detected by a biotinylated anti-IFNγ antibody and development with a streptavidin alkaline phosphatase and chromogenic substrate. Spots were analysed and counted using an automated plate reader (CTL Europe GmbH, Aalen, Germany).

ELISA Assay

Blood was collected from mice and allowed to clot for at least 30 minutes at room temperature, centrifuged at 1000g for 10 minutes and then sera collected. A naïve mouse serum sample was used as a control. Sera were diluted in 2% BSA-PBS and incubated for one hour at room temperature (RT) in coated S1 protein, N protein, Nunc Immuno plate F96 MaxiSorp ELISA plates, all at 200ng/well and then blocked with casein. S1 antibody binding was detected using a 3-step approach consisting of Goat-anti-mouse IgG Fc biotin followed by Streptavidin-HRPO conjugate and finally TMB (3,3´, 5, 5´- tetramethylbenzidine) core plus reagent (Bio-Rad BUF062C) for development. N antibody binding was detected using a 2-step approach where Goat pAb to mouse IgG (HRP) was used after the serum incubation step, followed by the development described

above. In both instances, once sufficiently developed, the reaction was stopped using 1M H_2SO_4 and the plates were read at 450 nm wavelength on a plate reader.

Histopathological analysis

Livers and kidneys were collected from each group for the histological and immunohistochemical studies and then tissues were perfused by 200 mL of paraformaldehyde (4%) in phosphate buffer saline (0.1M) for 48 hours. Then tissues were processed using alcohol series and Xylene. After 24 h, tissues were embedded in paraffin blocks and left at room temperature for overnight. Haematoxylin and eosin (H&E) and Terminal deoxynucleotidyl transferase dUTP nick-end labeling (TUNEL) staining were used for the paraformalin fixed tissue sections which were 10 µm. An Olympus C 5050 digital camera attached on an Olympus BX 51 microscope was used to record the sections. For the apoptotic cell percentage quantification of tissues QuPath software version 0.5.1 was used [30].

Statistical analysis

Graphs and statistics were prepared in GraphPad Prism 9.5.1 version or higher. Statistical differences were analysed using either one-way or two-way ANOVA adjusted for multiple comparison (either Tukey's or Dunnet's), p value lower than 0.05 was considered as statically significant and the levels of statistical significance were set $p^* < 0.05$, $p^{**} < 0.01$, $p^{***} < 0.001$ and $p^{****} < 0.0001$.

Results and Discussion

Synthesis and Characterisation of PBAEs

We initially synthesised an acrylate end-group terminated poly(beta-amino) ester derived from an aza-Michael addition polymerisation between 1,4-butanediol diacrylate (BDD) and 5-amino-1-pentanol (5AP) which could be used for post-functionalisation. This PBAE composition was chosen due to several previous pre-clinical studies indicating excellent formulation properties (particle size, stability, and zeta potential) as well as high transfection efficiencies both in vitro and in vivo across a range of nucleic acid cargos. Diacrylate and amine monomers were mixed then heated for 24 h at a ratio of 1.1:1 acrylate:amine (Figure 2A) to yield the base PBAE pBDD-5AP. ^{1}H-NMR spectroscopy indicated pBDD-5AP had the desired co-monomer composition and exhibited terminal acrylate groups required for post modification (Figure 2A). GPC analysis revealed a monomodal chromatogram with $Đ$ =1.3 and an average molar mass of 7700 g mol^{-1}. The pBDD-5AP PBAE was end-capped either with a further aza-Michael addition with 5-AP or via thiol-acrylate Michael addition with an 800 g mol^{-1} mono-thiolated PEG-to yield OH-(pBDD-5AP)-OH and PEG-(pBDD-5AP)-PEG (Figure 2B and Figure 2C). Full end-capping was confirmed with the disappearance of acrylate signals in the ^{1}H NMR spectra (Figure 2E). We observed a modest increase in molar masses for 5-AP end-capped polymers, reaching 8500 g mol^{-1} while the PEG terminated PBAEs exhibited a clear shift towards higher molar mass ($M_{n,th}$ = 12300 g mol^{-1}) due to PEG conjugation. Overall, all polymer characterisation confirmed the preparation of our targeted structures (Figure 2B).

The buffering capacities of OH-(pBDD-5AP)-OH and PEG-(pBDD-5AP)-PEG were evaluated by acid-base titration (over the pH range of 10.0–3.0) as pK_a of polycations has been suggested to

be important for facilitating endosomal buffering and endosomal escape of polymer based nucleic acid delivery systems [31, 32]. Both PEGylated and non-PEGylated PBAEs showed similar titration curves suggesting that PEGylation did not affect the buffering capacity (Figure 2D) thus any co-formulations between the OH-(pBDD-5AP)-OH and PEG-(pBDD-5AP)-PEG should have identical buffering capabilities.

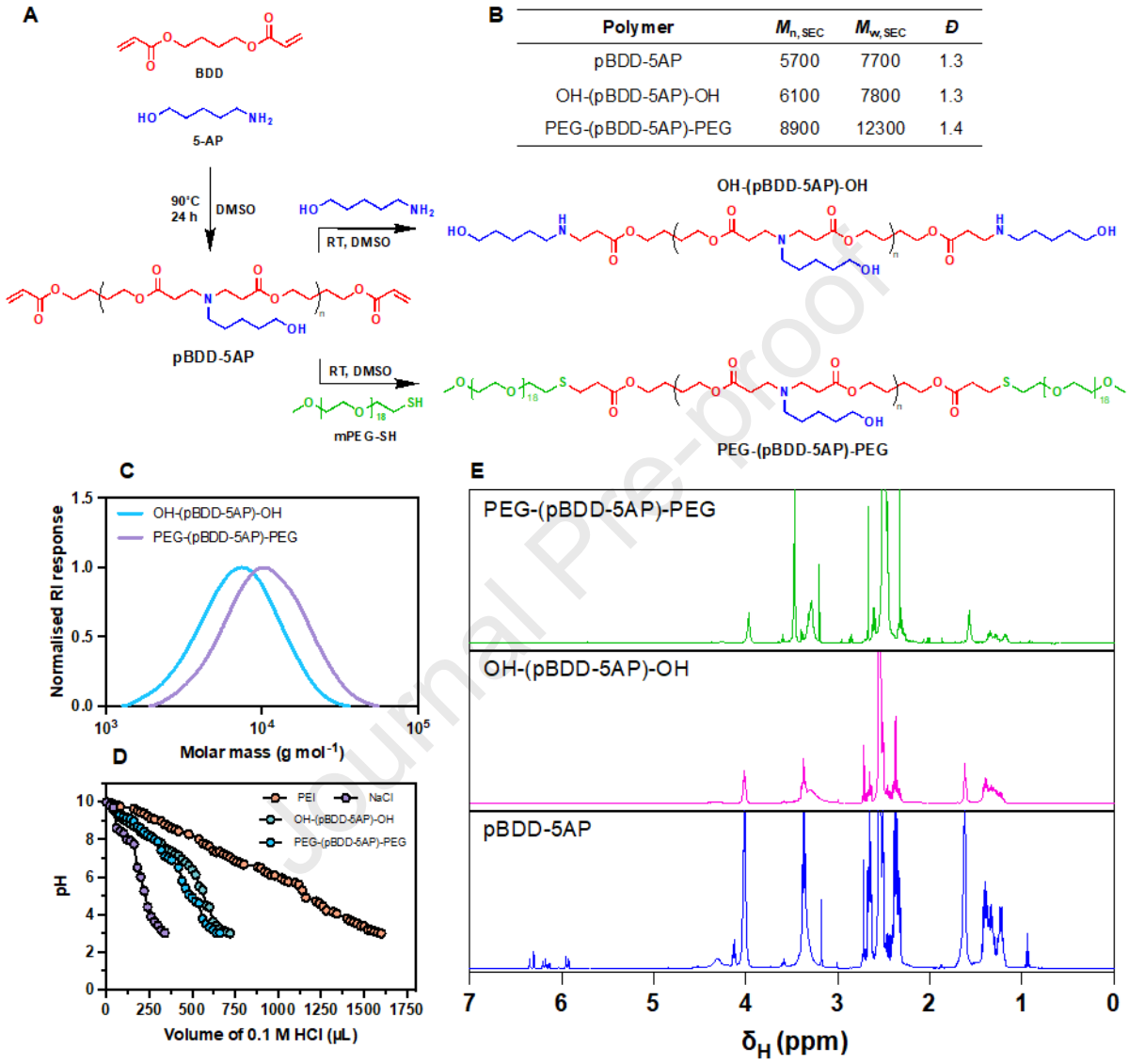

Polymer	$M_{n,SEC}$	$M_{w,SEC}$	$Đ$
pBDD-5AP	5700	7700	1.3
OH-(pBDD-5AP)-OH	6100	7800	1.3
PEG-(pBDD-5AP)-PEG	8900	12300	1.4

Figure 2. Synthesis and characterisation of PBAEs. (*A*) Synthetic scheme for step-growth Michael-addition polymerisation of BDD, 5-AP and mPEG-SH to produce PEG-PBAE-PEG triblock copolymer. First, acrylate-terminated base polymer was synthesised by polymerisation of monomer BDD and 5-AP. In the second step, base polymer was further terminated with 0.8 kDa mPEG-SH. (*B*) Molecular weights of PBAEs determined using GPC and (*C*) the molecular weight distribution of OH-(pBDD-5AP)-OH and PEG-(pBDD-5AP)-PEG. (*D*) Buffering capacity of OH-(pBDD-5AP)-OH and PEG-(pBDD-5AP)-PEG compared to polyethyleneimine (PEI) and negative control of a 0.1 M $NaCl_{(aq)}$ solution. (*E*) ^{1}H NMR spectra of pBDD-5APm OH-(pBDD-5AP)-OH showing disappearance of the acrylate peaks at 6-7 ppm indicating complete capping with either 5-amino-1-butanol for OH-(pBDD-5AP)-OH or PEG-SH for PEG-(pBDD-5AP)-PEG.

Effect of PEG Density on Polyplex Physicochemical Properties

Polyplex preparation was performed with three different polymer / fluc pDNA ratios weight-to-weight ratios (w/w ratios of 32, 64 and 128) for OH-(pBDD-5AP)-OH and PEG-(pBDD-5AP)-PEG PBAEs to optimise size, surface charge, encapsulation efficiency, biocompatibility, and DNA expression. To assess the effect of PEG density on the surface on the nanoparticle surface, we also prepared polyplexes prepared with a 1:1 weight:weight mixture of OH-(pBDD-5AP)-OH and PEG-(pBDD-5AP)-PEG, termed 'mix' (Figure 3A). This ratio represents a molar ratio of 2/3 PEG-(pBDD-5AP)-PEG/ OH-(pBDD-5AP)-OH and has been previously shown to be more effective at delivering siRNA in glioblastoma than the PEGylated or non-PEGylated formulations alone; however, has not been utilised in DNA vaccination [33].

Hydrodynamic diameters of all nanoparticles were observed to be between 100-150 nm with low polydispersity index (PDI) values (< 0.2) determined by dynamic light scattering (DLS) (Figure 3B), with no major changes in particle size observable across different w/w ratios. Notably, PEG-(pBDD-5AP)-PEG polyplexes produced smaller hydrodynamic diameters compared to OH-(pBDD-5AP)-OH non-PEGylated particles, suggesting that end modification of the polymer with mPEG-SH induced more compact structures in the final kinetically-trapped polyplexes, consistent with previous reports on PEGylated polyplexes [34]. In addition, zeta potentials of the particles were measured to be between 10-15 mV and no significant difference was observed between the groups (Figure 3C)**.** TEM micrographs of PEG-(pBDD-5AP)-PEG/pDNA polyplexes prepared at a w/w ratio of 64 showed the complexes to be spherical, and between 30 to 180 nm in diameter consistent with DLS analysis, albeit with particle shrinkage in the dry state for electron microscopy (Figure 3D, Figure 3E and Figure S1). Interestingly for the PEGylated and mixed polyplexes we observed a clear core-shell structure across most of the particles imaged, with a dark core and less electron dense corona attributable to the PEG surface. In contrast non-PEGylated polyplexes did not exhibit this core-shell morphology with only a single phase of electron dense core evident. We believe these TEM images and morphological differences evidence the absence or presence of PEG expressed on the surface of these polyplexes, in line with the formulations produced.

Furthermore, as DLS analysis is typically skewed towards larger particles it is likely any smaller species may be underrepresented in the overall sizes reported by light scattering. The presence of some free nucleic acids in agarose gel electrophoresis experiments for OH-(pBDD-5AP)-OH formulations indicated less complete complexation with the non-PEGylated material. In contrast, full incorporation of DNA was observed for the PEG-(pBDD-5AP)-PEG and mixed polyplexes (Figure 3F). Overall, these results indicate that all three formulations were capable of encapsulating pDNA with both the PEG-(pBDD-5AP)-PEG and mixed polyplexes offering smaller particle sizes and marginally higher pDNA encapsulation efficiency. To investigate the PEG surface density, a PEG-selective aggregation assay was conducted based on the well-established property of PEG as a tannin binding agent which occurs through hydrogen bonding [35]. This assay is similar to lectin-glycopolymer assays, where addition of multivalent lectin induces an increase in solution absorbance due to particle aggregation [36]. PEG-(pBDD-5AP)-PEG, OH-(pBDD-5AP)-OH, the mixed nanoparticles and sodium acetate buffer (as negative control) were subjected to tannic acid treatment, and absorbance at 500 nm was tracked using a UV-VIS spectrometer (Figure S2). There was no change for sodium acetate buffer after tannic acid addition. Some degree of increase was observed for the OH-(pBDD-5AP)-OH nanoparticles compared to sodium acetate buffer which could be due some interactions between the tannic acid and the highly hydroxylated polymer through hydrogen bonds. Notably, a rapid rise in absorbance at 500 nm was monitored upon treating PEG-(pBDD-5AP)-PEG nanoparticles with tannic acid suggesting high availability of PEG in their surface. And finally, the degree of aggregation for mixed nanoparticles was at a level between those for PEGylated and non-PEGylated nanoparticles suggesting availability of PEG at the surfaces of the mixed nanoparticles was also at an intermediate level compared to the fully PEGylated and non-PEGylated systems.

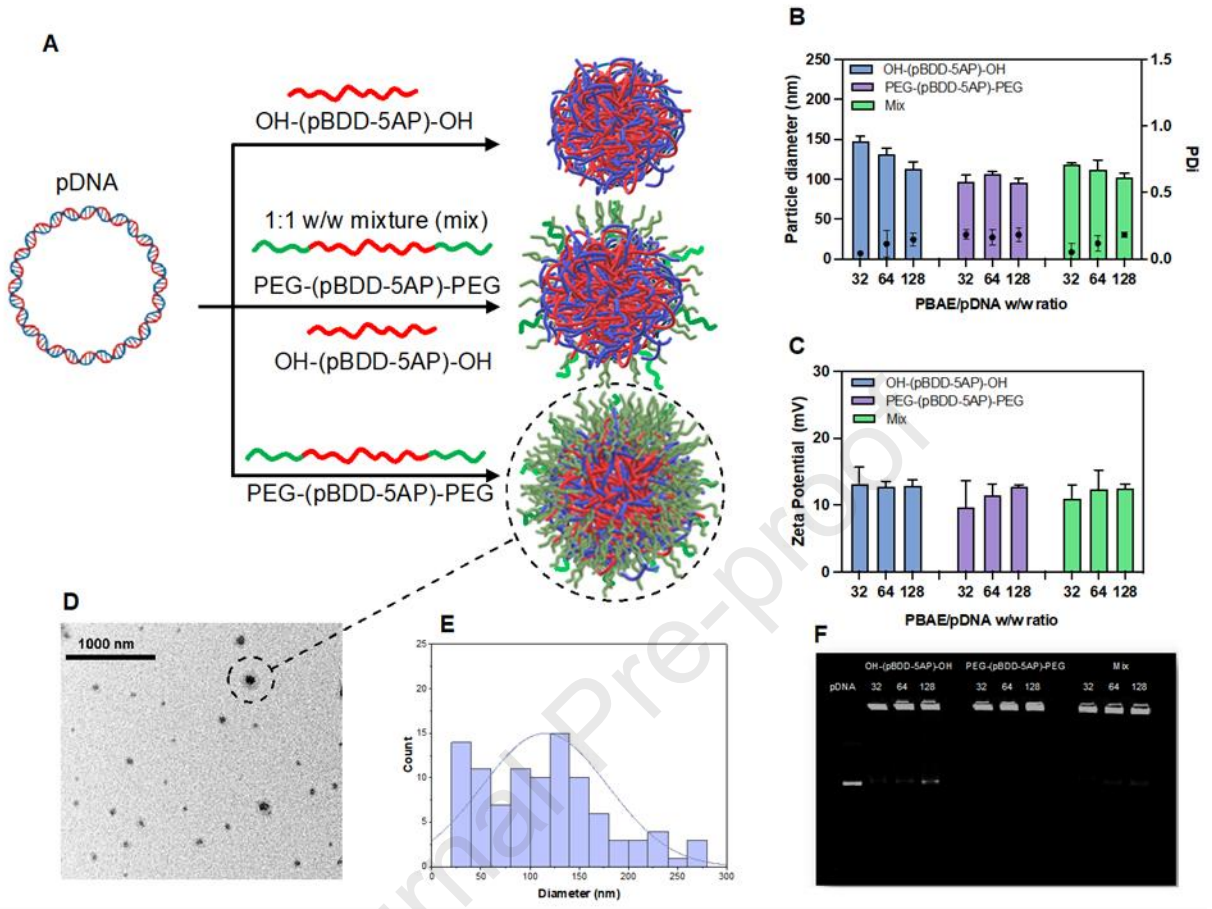

Figure 3. Formulation of PBAEs with pDNA to produce polyplex nanoparticles. (*A*) Schematic representation of pDNA formulation with OH-(pBDD-5AP)-OH, PEG-(pBDD-5AP)-PEG or a 1:1 w/w mixture of OH-(pBDD-5AP)-OH, PEG-(pBDD-5AP)-PEG termed 'mix' in pH 5.0 25 mM sodium acetate at a final pDNA concentration of 10 µg/mL. (*B*) Particle size and (*C*) Zeta potential for the OH-(pBDD-5AP)-OH, PEG-(pBDD-5AP)-PEG and 'mix' polyplexes at a PBAE/pDNA w/w ratio of 32, 64 and 128 determined by dynamic light scattering at 25˚C. Bars represent the mean ± SD for 3 independent formulations. (*D*) Representative transmission electron micrograph of PEG-(pBDD-5AP)-PEG polyplexes (scale bar corresponds to 1000 nm) and (*E*) measured particle size distribution from five separate TEM images. (*F*) Encapsulation efficiency of pDNA within polyplexes evaluated using agarose gel retardation assay.

In Vitro Evaluation of pDNA Delivery

The acute toxicity and pDNA delivery efficiency of the individual OH-(pBDD-5AP)-OH, PEG-(pBDD-5AP)-PEG was examined in HEK293T and DC2.4 cells as a model and vaccine relevant dendritic cell line respectively. Similar to the formulation characterisation study above, polyplexes were prepared at polymer/pDNA w/w ratios of 32, 64, and 128 utilising a firefly luciferase encoding pDNA and compared against lipofectamine (positive expression control) and Triton X-100 (positive toxicity control). All the formulations exhibited more than 50% cell viability and, in general, DC2.4 cells displayed high metabolic activity compared to HEK293T cells which may be due to the lower transfectability of the dendritic cells (Figure 4A and Figure 4B) [37]. Similar to previous studies, increasing w/w ratio resulted in increased toxicity due to increased polycation concentration which is known to disrupt the negative phospholipid bilayer [38]. Interestingly, a significant difference was observed for the mixed and PEG-(pBDD-5AP)-PEG formulation in the DC2.4 cell line with cell viability around 50% and 94% for w/w 128 and w/w 64, respectively

(Figure 4A and Figure 4B). Notably, formulations prepared at higher w/w ratios yielded greater transfection efficacy often exceeding the luciferase expression of the lipofectamine positive control (Figure 4C and Figure 4D). Unlike in HEK293T cells the OH-(pBDD-5AP)-OH formulations did not show statistically significantly higher luciferase expression than naked pDNA in DC2.4 cells, yet both the mixed and PEG-(pBDD-5AP)-PEG derived polyplexes yielded increased pDNA expression in the DC2.4 cells. This could be due to the above-mentioned compact structure of PEGylated formulations where the diameter of nanoparticles was observed to be smaller than that of non-PEGylated ones, and thus, above shown increased nucleic acid encapsulation. This phenomenon may also be the result of PEG shielding the dsDNA from cytosolic DNA sensors which are present in the DC2.4 cells but not HEK293 cells thus initiating a type-1 interferon response and inhibiting downstream RNA translation and thus expression of the luciferase reporter [39]; however, this would require further investigation.

Membrane interactions of the formulations were evaluated via propensity to lyse RBCs compared to NaOAc buffer (negative control, NC) and Triton-X (positive control, PC). It was found that, as the w/w ratio of particles increased, a higher level of haemolytic activity was observed, in agreement with previous studies [40]. In addition, PEGylation significantly decreased the haemolytic activity of the formulations with w/w 128 (**$p < 0.01$) and W/W 64 (*$p < 0.05$) ratios (Figure S3). This is likely due to decreased surface charge of PEGylated formulations thus decreased interactions between negatively charged RBCs and positively charged polymers [41]. The tolerability of these polyplexes were also further evaluated in assays measuring cell viability of mouse derived BM DCs treated with the polyplexes (Figure S4). As GM-CSF, a growth stimulating factor for dendritic cells as well as other myeloid cells, was used in this culture, an optimised gating strategy was needed to identify solely dendritic cells. In order to do this, cells were gated on live, $CD45^{pos}$, $Ly6c^{low}$ $B220^{low}$, $CD11c^{pos}$, MHC II^{pos} (Figure S5). The dendritic cells, when transfected with all formulations showed no significant change in live cell count in comparison to the dendritic cells that were not transfected. This demonstrates that our PBAE derived polyplexes do not affect the viability of dendritic cells *in vitro.*

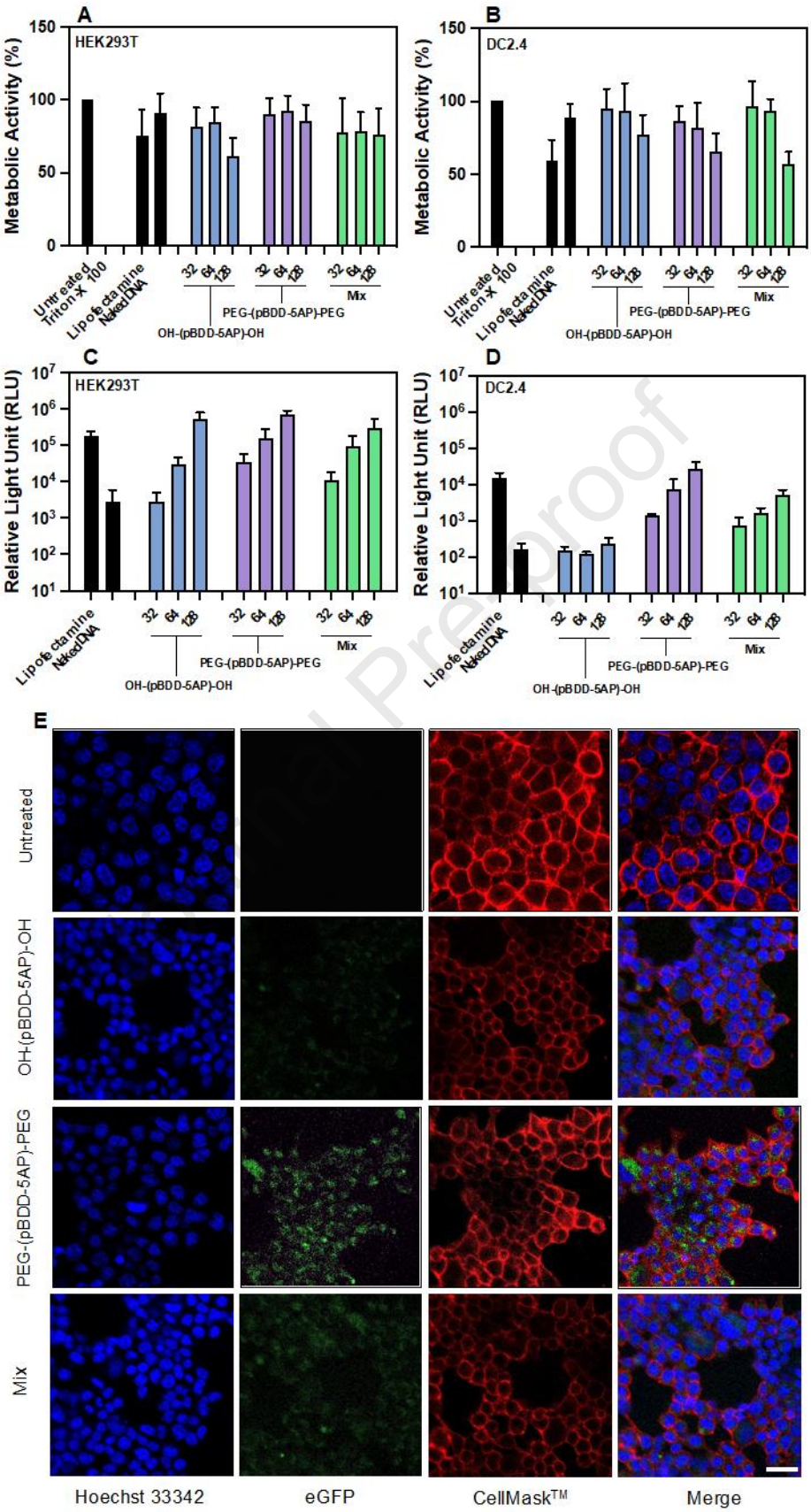
A
HEK293T
Metabolic Activity (%)
150
100
50
0
Untreated
Triton-X 100
Lipofectamine
Naked DNA
32
64
128
Mix
PEG-(pBDD-5AP)-PEG
OH-(pBDD-5AP)-OH
B
DC2.4
C
HEK293T
Relative Light Unit (RLU)
D
DC2.4
E
Untreated
OH-(pBDD-5AP)-OH
PEG-(pBDD-5AP)-PEG
Mix
Hoechst 33342
eGFP
CellMask™
Merge

Figure 4. Metabolic activity and transfection efficiency of PBAE derived pDNA polyplexes. Effect of PBAE polyplexes formulated with firefly luciferase encoding pDNA at PBAE/pDNA w/w ratios of 32, 64 and 128 on metabolic activity (*A* and *B*) and transfection efficiency (*C* and *D*) on HEK293T cells (*A* and *C*) and DC2.4 cells (*B* and *D*). Cells were treated with polyplexes containing pDNA at a concentration of 500 ng/mL (100 ng/well) in serum-free Opti-MEM. Metabolic activity was compared against Triton X (positive control) and untreated cells (negative control), and calculated by normalizing metabolic activity to untreated cells. In vitro transfection efficiency was analysed after 24 h post-transfection using the Promega ONE-GLO luciferase assay and compared against Lipofectamine 2000 (positive control) and naked pDNA (negative control) expressed as relative light units (RLU) for luciferase expression. Bars represent the mean ± SD. (*E*) Representative live cell confocal microscopy images of HEK293T cells 4 h post-transfection with an eGFP encoding pDNA formulated with OH-(pBDD-5AP)-OH, PEG-(pBDD-5AP)-PEG or a 1:1 w/w mixture of OH-(pBDD-5AP)-OH and PEG-(pBDD-5AP)-PEG termed 'mix' at a PBAE/pDNA w/w ratio of 64. Cells were stained with Hoechst 33342 CellMask™ Plasma Membrane Stain Deep Red to visualise the nucleus and cell membrane respectively. Images are displayed as individual channels and a merged signal. Scale bar corresponds to 20 µm (x40). Note: the contrast of the images has been enhanced for clarity, original images can be found in the supporting information (Figure S6).

Due to the encouraging results with all three formulations at w/w 64 exhibiting high luciferase expression and minimal reduction in metabolic activity, we further investigated these formulations for pDNA expression with live cell confocal microscopy. All polymers were formulated with GFP-encoding pDNA and exposed to HEK293T cells for four hours. Following incubation, green fluorescence attributed to GFP expression could be observed within the cytosol indicating successful transfection (Figure 4E).

To evaluate the cellular association of PEG-(pBDD-5AP)-PEG (w/w 64) polyplexes in DC2.4 cells, we first generated a FITC labelled PEG-(pBDD-5AP)-PEG by conjugating FITC on to the pendant hydroxyl groups of the core PBAE. Cellular uptake was assessed through imaging flow cytometry, a single cell microscopy technique at 30 min, 1 h, 2 h, and 4 h after treatment (Figure 5A). It was observed that 97.8% of DC2.4 cells were FITC-positive indicating successful cell association within 1 hour of incubation. There was a further increase to 99.5% FITC-positive at both 2 h and 4 h incubation times overall highlighting rapid association of the administered polyplexes. Notably the median fluorescence intensity rose from 4500 arbitrary units up to 18400 between 30 min and 4 h incubation, indicating an initial rapid uptake by the DC2.4 cells which continued throughout the course of the experiment. Compared to traditional flow cytometry the images from each cell can be analysed to compare internalisation vs membrane association. The median of internalisation score of the polyplexes was approximately 1.4 indicating a high proportion of nanoparticles were internalised inside the cells since having a score less than 0.3 can be considered to be surface bound (Figure 5A, B and C) [42].

To further assess the intracellular internalisation mechanism of the PEG-(pBDD-5AP)-PEG in DC2.4 cells we employed confocal microscopy to evaluate colocalization with a lysosomal (Lysotracker™ red) and nuclear (Hoecht 33342) stain (Figure 5D). After 1 and 4 h post administration, confocal micrographs showed that polyplexes successfully internalised within dendritic cells and merged images demonstrated with minimal co-localisation with the acidic lysosomes with image analysis indicating Pearson's Correlation Coefficient between FITC labelled polyplexes and Lysotracker™ stained lysosomes were below 0.5 (Table S1). Given the ~100 nm particle diameters it is likely that these formulations will be uptaken by endocytosis, however the minimal colocalization with the acidic lysosomes may indicate successful escape a the before endosomal maturation in lysosomes compartments. Although further endosomal escape studies would be needed to fully investigate this phenomenon, it is likely this feature heavily explains the high expression efficiencies observed, as endosomal escape is one of the key bottlenecks in cytosolic gene and drug delivery.

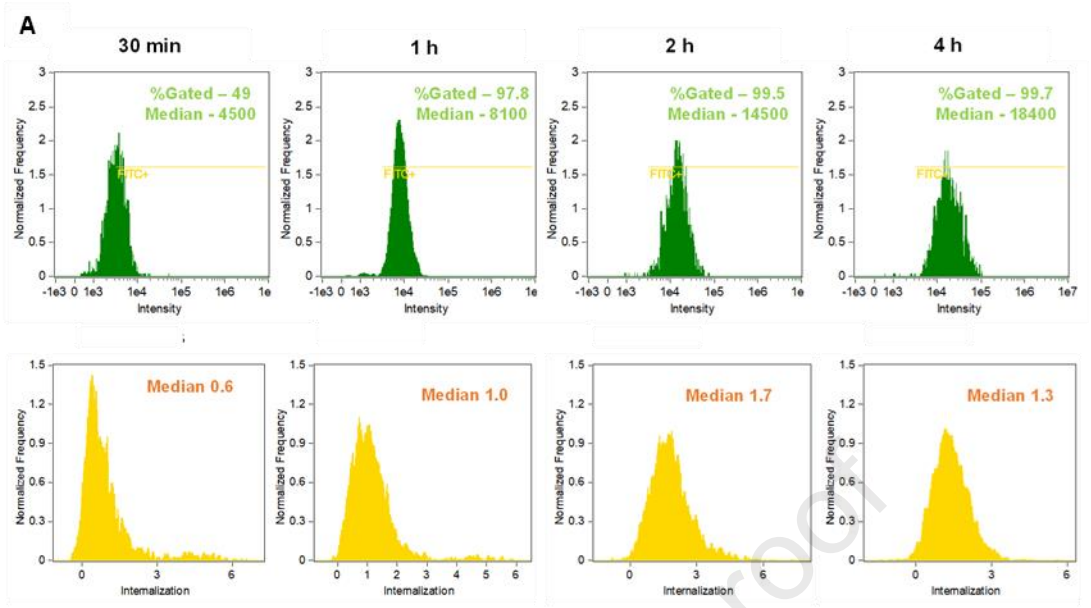
A
30 min
1 h
2 h
4 h
%Gated – 49
Median - 4500
%Gated – 97.8
Median - 8100
%Gated – 99.5
Median - 14500
%Gated – 99.7
Median - 18400
Normalized Frequency
Intensity
Median 0.6
Median 1.0
Median 1.7
Median 1.3
Internalization

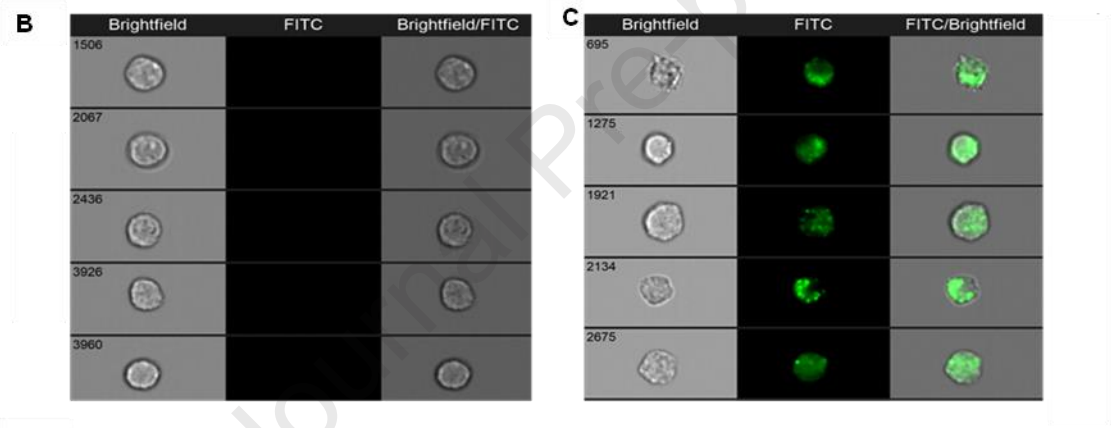
B
Brightfield
FITC
Brightfield/FITC
1506
2067
2436
3926
3960
C
Brightfield
FITC
FITC/Brightfield
695
1275
1921
2134
2675

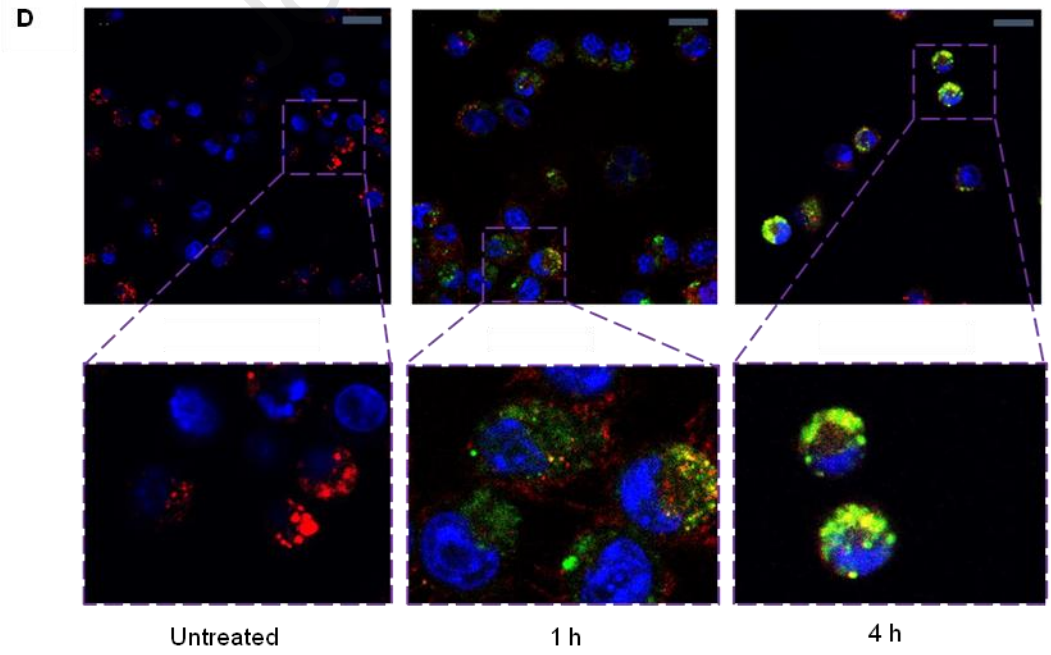
D
Untreated
1 h
4 h

Figure 5. Cellular uptake of PBAE derived pDNA polyplexes. (*A*-*C*) Imaging cytometry (*A*) histograms of fluorescence intensity and internalisation for DC2.4 cells after 30 mins, 1 h, 2 h and 4 h following treatment with FITC-labelled PEG-(pBDD-5AP)-PEG polyplexes at a PBAE/pDNA w/w ratio of 64 at 500 ng/mL pDNA. Untreated fluorescence intensity histogram can be found in the supporting information (Figure S7) Data were analysed using IDEAS software. (*B* and *C*) Representative images for imaging cytometry for untreated and treated group after 4 h *(D)* Representative merged live cell confocal microscopy images of DC2.4 cells treated pDNA polyplexes derived from FITC-labelled PEG-(pBDD-5AP)-PEG at a PBAE/pDNA w/w ratio of 64 after 1 h and 4 h at 100 ng/well (500 ng/mL) pDNA. Scale bar 10 µm (40x). Note: the contrast of the images has been enhanced for clarity, original images can be found in the supporting information (Figure S8).

In Vivo Delivery of a SARS-CoV-2 Bivalent pDNA Vaccine

Due to the encouraging in vitro pDNA expression and polyplex uptake in DC2.4 cells we hypothesised that these materials may be effective in delivering a pDNA vaccine against infectious disease. We therefore evaluated antigen specific T-cell responses of our formulations encapsulating a bivalent pDNA vaccine, encoding for both the nucleocapsid and spike protein of SARS-CoV-2 [43]. This construct has previously shown positive neutralising antibody titres ixn vivo following jet injector administration, however there is a need for more accessible delivery technologies for this vaccine candidate. Genomic studies on SARS-CoV-2 evolution have indicated that mutation in the spike (S1) protein is the predisposing factor to waning vaccine immunity against new variants. Therefore, a vaccine inducing expression of the nucleocapsid (N) protein may have advantages for future protection against SARS-CoV-2 infections (a “variant-agnostic”) vaccine as the nucleocapsid features are relatively well conserved between variants [44].

We therefore produced polyplexes derived from OH-(pBDD-5AP)-OH, PEG-(pBDD-5AP)-PEG and the 1:1 w/w mixture between these polymers, termed ‘mix’ at a PBAE/pDNA w/w ratio of 64 using the SARS-CoV-2 bivalent pDNA vaccine. these polyplexes were then investigated for their ability to deliver the bivalent SARS-CoV-2 DNA vaccine. 3 groups of female Balb/C mice were injected intramuscularly with a 5 µg pDNA dose and compared against a positive control of 1 µg pDNA vaccine delivered via gene gun. Doses were administered in a prime-boost regime, with 3 identical im injections spaced 7 days apart (Figure 6A). Serum was collected at day 21 post-immunisation and then the mice were euthanised for spleen harvest, to evaluate whether any bivalent SARS-CoV-2 pDNA PBAE-formulated vaccines could induce spike and nucleocapsid T cell immune responses after booster doses. No adverse effects were observed during the course of the animal experiment, with body weights of the animals remaining relatively constant and no animals requiring removal from the study (Figure 6D).

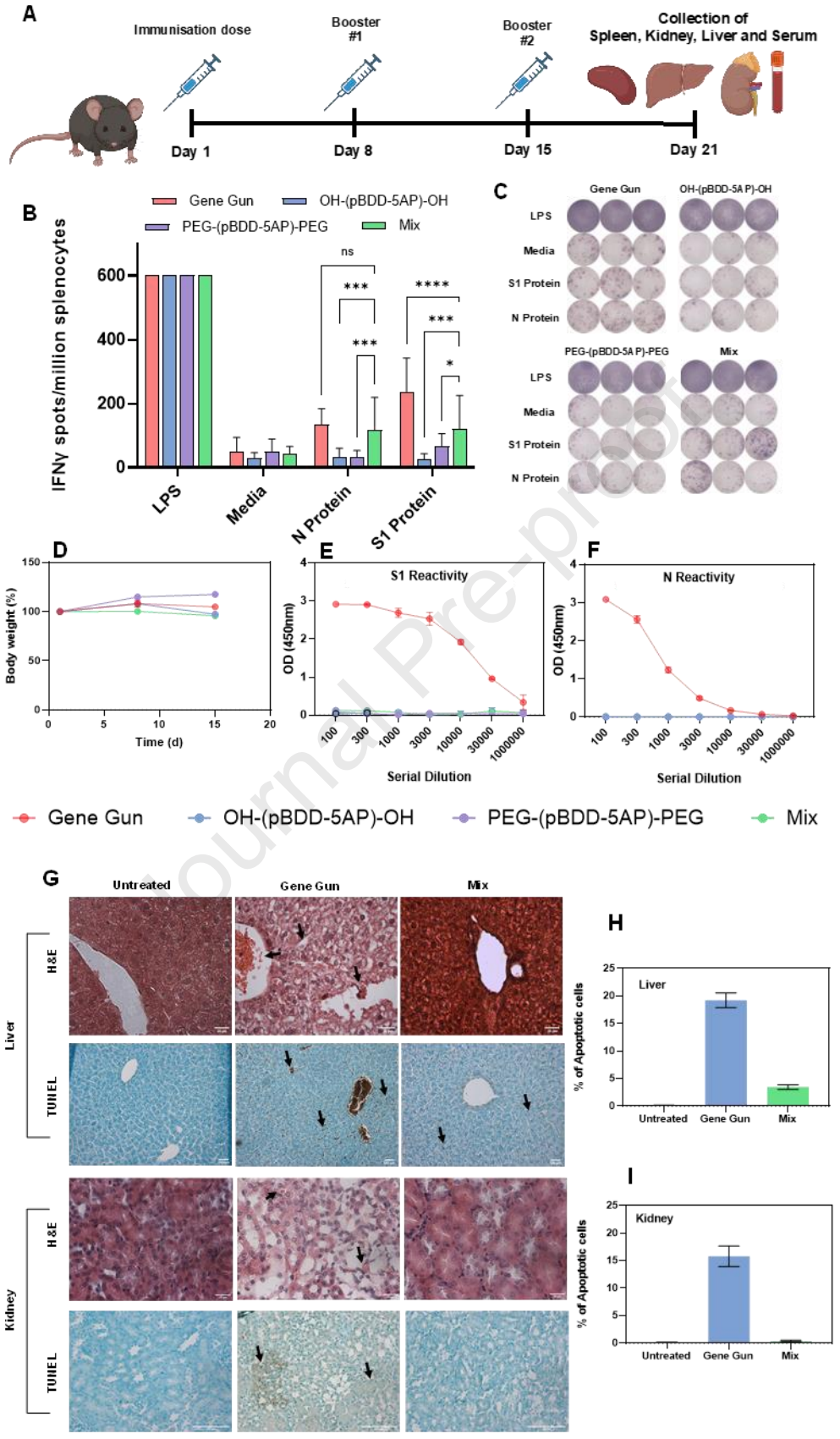
A
Immunisation dose
Booster #1
Booster #2
Collection of Spleen, Kidney, Liver and Serum
Day 1
Day 8
Day 15
Day 21
B
Gene Gun
OH-(pBDD-5AP)-OH
PEG-(pBDD-5AP)-PEG
Mix
IFNγ spots/million splenocytes
LPS
Media
N Protein
S1 Protein
C
Gene Gun
OH-(pBDD-5AP)-OH
PEG-(pBDD-5AP)-PEG
Mix
LPS
Media
S1 Protein
N Protein
D
Body weight (%)
Time (d)
E
S1 Reactivity
OD (450nm)
Serial Dilution
F
N Reactivity
OD (450nm)
Serial Dilution
Gene Gun
OH-(pBDD-5AP)-OH
PEG-(pBDD-5AP)-PEG
Mix
G
Untreated
Gene Gun
Mix
Liver
H&E
TUNEL
Kidney
H&E
TUNEL
H
Liver
% of Apoptotic cells
Untreated
Gene Gun
Mix
I
Kidney
% of Apoptotic cells
Untreated
Gene Gun
Mix

Figure 6. In vivo transfection, immunisation performance and tolerability following intramuscular administration of PBAE polyplexes containing a SARS-CoV-2 bivalent pDNA vaccine. *(A)* Schematic of the dosing schedule. *(B)* Antigen-specific T cell responses were quantified by IFN-γ ELISpot with splenocytes isolated from vaccinated mice 21 days following intramuscular administered 5 µg pDNA bivalent SARS-CoV-2 vaccine (encoding for both spike (S1) and nucleocapsid (N) proteins) complexed with OH-(pBDD-5AP)-OH, PEG-(pBDD-5AP)-PEG or a 1:1 w/w mixture of OH-(pBDD-5AP)-OH and PEG-(pBDD-5AP)-PEG termed 'mix' at a PBAE/pDNA w/w ratio of 64. These were compared against a positive control of gold particle associated gene gun delivered vaccine. Doses were administered in a prime-boost regime, with 3 identical injections spaced 7 days apart. *(C)* Representative images of IFN-γ spot-forming cells *(D)* Animal body weight data over the time course of the experiment. *(E)* Serum N and *(F)* S1 antibody response 21 d after vaccination as determined by an ELISA assay. *(G)* Histopathological analysis of liver and kidney to investigate tissue damage for the non-treated, positive control and 'mix' polyplexes. H&E and TUNEL staining was utilised for the analyses of general tissue structure and apoptotic cells respectively. Scale bar 20 µm and 100 µm for H&E and TUNEL images respectively the percentage of apoptotic cells in the (*H*) liver and (*I*) kidney histopathology was quantified using QuPath software. Bars represent the mean ± standard deviation. Statistical analyses were performed with a two-way ANOVA with Tukey multiple comparisons post-hoc test with level of statistical significance represented as $p^* < 0.05$, $p^{**} < 0.01$, $p^{***} < 0.001$ and $p^{****} < 0.0001$.

The levels of antigen specific T-cells were investigated by evaluating the IFNγ expression via an ELISpot assay performed on splenocytes harvested from vaccinated mice. Gene gun vaccinated mice elicited the highest IFNγ secretion when stimulated with both N and S1 proteins ($p < 0.0001$ against media control). In contrast there was no statistically significant ($p > 0.05$ against media control) T-cell IFN γ expression after stimulation with the N and S1 proteins for the OH-(pBDD-5AP)-OH and PEG-(pBDD-5AP)-PEG polyplexes (Figure 6B and Figure 6C) compared to non-stimulated splenocytes, despite the PEGylated PBAE yielding the highest in vitro transfection performance in DC2.4s**.** Surprisingly we observed excellent IFNγ secretion for the sparsely PEGylated, mixed polyplexes, with equivalent and 70% spot formation compared to the gene gun positive control for the S1 protein and N protein respectively (Figure 6B, Figure 6C). The reasons for this enhanced efficacy, and importantly poor correlation between the in vitro and in vivo experiments are not immediately clear, however it is possible that modulation of PEG density may attenuate immunogenic response or improve diffusion of the formulations beyond the injection site.

ELISA assays were performed with collected serum samples at day 21 to detect N and S1 antibody reactivity. Serial dilutions of positive control gene gun serum indicated potent reactivities suggesting the positive control immunisation stimulates strong antibody responses to both the nucleocapsid and spike proteins, consistent with previous data [29]. However, none of the PBAE formulations stimulated detectable antibody responses despite evidence of N and S1 protein expression in the mixed PBAE formulation (Figure 6E, Figure 6F). This may be due to the reduced DNA dose compared to previous DNA vaccine studies, and may not be an adequate dose to stimulate antibody responses despite initiating protein expression or poor adjuvanticity of the formulation [45]. The limited antibody response may also be related to quantity of DNA taken up by antigen presenting cells or trafficked to lymph nodes being higher from gene gun, than from the PBAE formulations. Recent findings have suggested that inclusion of lipophilic side chain monomers into PBAEs may improve transfection of dendritic cells, hence could be an area of exploration for DNA vaccine polymer formulations in future [46].

The improved safety profile of new vaccine excipients and technologies is of utmost importance, particularly given recent reports on autoimmune hepatic injury following SARS-CoV-2 vaccination [47]. Accordingly, histological analysis of the liver was conducted from mice at the end of the vaccination study. We observed that the liver architecture and components of the mixed formulation were similar to those of the non-treated group, whereas enlarged interhepatic plate spaces and endothelial cells were distinct in the liver tissue in the gene gun treated group (Figure 6G). The highly loaded blood vessels may also indicate severe inflammation for the positive control group, which again was not observed for the mixed formulations. Similarly, the findings for the H&E-stained kidney tissue architecture and the components were close to non-treated group

compared to the ‘mix’ formulation. Finally, the vaccine induced inflammatory response may initiate apoptotic mechanisms in these cells, hence apoptosis was investigated via a TUNEL assay and then the data was analysed using QuPath software to quantify this. As expected, liver and kidney sections from untreated mice displayed minimal apoptosis, and a similarly low level of apoptosis was observed for the mixed formulation. In contrast the positive gene gun control displayed several apoptotic regions and thus high apoptotic cell percentage quantified by QuPath (Figure 6H and Figure 6I). The higher inflammatory and apoptotic features observed for the positive control, compared to the PBAE formulations may be correlated with their greater antibody responses.

Taken together, the results from this work indicate that PEGylation of PBAEs plays a strong role in the in vitro and in vivo delivery efficiency of pDNA vaccines. Given the relatively similar physicochemical properties between PEGylated, non-PEGylated and mixed polyplexes it is unlikely this is the driving force in the enhanced activity seen for the PEGylated derivatives in the DC2.4 cell line. Previous studies on PBAEs have shown that high transfections efficiencies are typically achievable with polyplex nanoparticles of diameters below 200 nm [48], however the size alone does not guarantee efficacy, with monomer choice for the base PBAE critical for activity. Furthermore, the 3-4 orders of magnitude decrease in luciferase expression between the HEK293Ts and DC2.4 for the OH-(pBDD-5AP)-OH polyplexes, which was not as extensive for PEGylated derivatives, hints that shielding the dense positive charge on the polyplex surface may enhance the downstream intracellular pathways that are important in pDNA delivery or expression. For instance, it has previously been observed that the membrane disruptive nature of polycations can stimulate intracellular inflammatory pathways which may inhibit DNA transcription or mRNA translation as a defence to viral replication [49]. Such innate responses are more functional in immune cells than in HEK293Ts potentially explaining the differences observed between cell lines [50], The screening of positive charge may therefore explain why PEGylated PBAE polyplexes improve DNA expression, despite previous literature indicating that PEGylation drastically reduces uptake and therefore expression of nucleic acid formulations [51]. In contrast, the greater efficacy of the sparsely PEGylated ‘mix’ formulation in vivo may be explained by the known ability for PEGylated materials to diffuse further from the injection site, whilst potentially stimulating a moderate immunogenic response through weaker membrane interactions. As our markers for efficacy in the in vivo assay were related to vaccine response rather than antigen expression alone, this could result in enhanced activity for the ‘mixed’ formulation, while the PEGylated material does not stimulate a strong enough immune response, while the non-PEGylated derivative may yield an inflammatory response thus inhibiting the expression of the antigen.

Conclusions

In conclusion, in this work we demonstrate the role of PEGylation density in the formulation and delivery of pDNA in a vaccine relevant setting. Polyplexes derived from solely the PEG-(pBDD-5AP)-PEG or the 1:1 w/w mixture between PEG-(pBDD-5AP)-PEG and OH-(pBDD-5AP)-OH displayed smaller particle sizes, high encapsulation efficiencies and high transfectability of reporter pDNA constructs in HEK293T cells and importantly dendritic cells displaying their potential in vaccination. In further in vivo studies with a bivalent SARS-CoV-2 pDNA vaccine, only the mixed polyplex formulations demonstrated IFNγ similar to the gene gun positive control; however, did not exhibit any antibody response. The findings in this study suggest that polymer delivery systems are a promising avenue for DNA vaccines with the surface properties of polyplexes eliciting a strong role in the performance of these delivery systems. However future research should focus on routes to improve the quality of immune response achieved from these

vaccines when administered with polymer vectors. There is also significant scope to identify which polymer properties can tailor towards antibody or T-cell response, the main effectors in infectious disease vaccines and immunotherapies respectively.

Acknowledgements

We thank the Royal Society [Wolfson Research Merit Award WM150086 to CA]. Work on this project is supported by Wellcome Leap as part of the R3 Program [Biofoundry-in-a-Box] and Turkish Ministry of National Education. We also thank Tom Hyde, Esme Ireson and Paul Cooling for expert technical support. The Nanoscale & Macroscale Research Centre (NMRC) is acknowledged for providing the facilities for TEM and related analysis particularly to Denise McLean. We thank the School of Life Sciences imaging facility (SLIM) and their staff for use of their facilities. Elements of Figures 1 and 3 were Created with BioRender.com.

Data access statement

All relevant data can be obtained upon request from the corresponding authors at p.gurnani@ucl.ac.uk and cameron.alexander@nottingham.ac.uk

Conflict of Interest

We would like to disclose that P.S. and V.A.B. are employed by Scancell Limited and L.G.D is a director and shareholder of Scancell Ltd.

References

[1] J.R. Mascola, A.S. Fauci, Novel vaccine technologies for the 21st century, Nature Reviews Immunology 20(2) (2020) 87-88.

[2] A.J. Pollard, E.M. Bijker, A guide to vaccinology: from basic principles to new developments, Nature Reviews Immunology 21(2) (2021) 83-100.

[3] M.A. Kutzler, D.B. Weiner, DNA vaccines: ready for prime time?, Nature Reviews Genetics 9(10) (2008) 776-788.

[4] J. Lee, S.A. Kumar, Y.Y. Jhan, C.J. Bishop, Engineering DNA vaccines against infectious diseases, Acta Biomaterialia 80 (2018) 31-47.

[5] S. Liu, S. Wang, S. Lu, DNA immunization as a technology platform for monoclonal antibody induction, Emerging microbes & infections 5(1) (2016) 1-12.

[6] M.A. Liu, A Comparison of Plasmid DNA and mRNA as Vaccine Technologies, Vaccines 7(2) (2019) 37.

[7] D. Luo, W.M. Saltzman, Synthetic DNA delivery systems, Nature Biotechnology 18(1) (2000) 33-37.

[8] N.Y. Sardesai, D.B. Weiner, Electroporation delivery of DNA vaccines: prospects for success, Current Opinion in Immunology 23(3) (2011) 421-429.

[9] C. Ledesma-Feliciano, R. Chapman, J.W. Hooper, K. Elma, D. Zehrung, M.B. Brennan, E.K. Spiegel, Improved DNA Vaccine Delivery with Needle-Free Injection Systems, Vaccines 11(2) (2023) 280.

[10] E.S. Bergmann-Leitner, W.W. Leitner, Vaccination Using Gene-Gun Technology, Springer New York2015, pp. 289-302.

[11] T. Momin, K. Kansagra, H. Patel, S. Sharma, B. Sharma, J. Patel, R. Mittal, J. Sanmukhani, K. Maithal, A. Dey, H. Chandra, C.T.M. Rajanathan, H.P.R. Pericherla, P. Kumar, A. Narkhede, D. Parmar, Safety and Immunogenicity of a DNA SARS-CoV-2 vaccine (ZyCoV-D): Results of an open-label, non-randomized phase I part of phase I/II clinical study by intradermal route in healthy subjects in India, eClinicalMedicine 38 (2021).

[12] T. Travieso, J. Li, S. Mahesh, J.D.F.R.E. Mello, M. Blasi, The use of viral vectors in vaccine development, npj Vaccines 7(1) (2022) 75.

[13] B. Fayed, J. Jagal, R. Cagliani, R.A. Kedia, A. Elsherbeny, H. Bayraktutan, G. Khoder, M. Haider, Co-administration of amoxicillin-loaded chitosan nanoparticles and inulin: A novel strategy for mitigating antibiotic resistance and preserving microbiota balance in Helicobacter pylori treatment, International Journal of Biological Macromolecules 253 (2023) 126706.

[14] A. Elsherbeny, H. Bayraktutan, U.C. Oz, C. Moloney, J.C. Ashworth, A.M. Grabowska, C. Alexander, Responsive Nanomaterial Delivery Systems for Pancreatic Cancer Management, Advanced Therapeutics (2023) 2300330.

[15] Z.A. Azrak, M.S. Taha, J. Jagal, A. Elsherbeny, H. Bayraktutan, M.H. AbouGhaly, A.H. Elshafeey, K. Greish, M. Haider, Optimized mucoadhesive niosomal carriers for intranasal delivery of carvedilol: A quality by design approach, International Journal of Pharmaceutics (2024) 123935.

[16] R. Kumar, C.F. Santa Chalarca, M.R. Bockman, C.V. Bruggen, C.J. Grimme, R.J. Dalal, M.G. Hanson, J.K. Hexum, T.M. Reineke, Polymeric Delivery of Therapeutic Nucleic Acids, Chemical Reviews 121(18) (2021) 11527-11652.

[17] D.W. Pack, A.S. Hoffman, S. Pun, P.S. Stayton, Design and development of polymers for gene delivery, Nature reviews Drug discovery 4(7) (2005) 581-593.

[18] N.K. Dastgerdi, N. Gumus, H. Bayraktutan, D. Jackson, K. Polra, P.F. McKay, F. Atyabi, R. Dinarvand, R.J. Shattock, L. Martinez-Pomares, Charge neutralized poly (β-amino ester) polyplex nanoparticles for delivery of self-amplifying RNA, Nanoscale Advances (2024).

[19] X. Hou, T. Zaks, R. Langer, Y. Dong, Lipid nanoparticles for mRNA delivery, Nature Reviews Materials 6(12) (2021) 1078-1094.

[20] L.R. Baden, H.M. El Sahly, B. Essink, K. Kotloff, S. Frey, R. Novak, D. Diemert, S.A. Spector, N. Rouphael, C.B. Creech, J. McGettigan, S. Khetan, N. Segall, J. Solis, A. Brosz, C. Fierro, H. Schwartz, K. Neuzil, L. Corey, P. Gilbert, H. Janes, D. Follmann, M. Marovich, J. Mascola, L. Polakowski, J. Ledgerwood, B.S. Graham, H. Bennett, R. Pajon, C. Knightly, B. Leav, W. Deng, H. Zhou, S. Han, M. Ivarsson, J. Miller, T. Zaks, Efficacy and Safety of the mRNA-1273 SARS-CoV-2 Vaccine, New England Journal of Medicine 384(5) (2021) 403-416.

[21] F.P. Polack, S.J. Thomas, N. Kitchin, J. Absalon, A. Gurtman, S. Lockhart, J.L. Perez, G. Pérez Marc, E.D. Moreira, C. Zerbini, R. Bailey, K.A. Swanson, S. Roychoudhury, K. Koury, P. Li, W.V. Kalina, D. Cooper, R.W. Frenck, L.L. Hammitt, Ö. Türeci, H. Nell, A. Schaefer, S. Ünal, D.B. Tresnan, S. Mather, P.R. Dormitzer, U. Şahin, K.U. Jansen, W.C. Gruber, Safety and Efficacy of the BNT162b2 mRNA Covid-19 Vaccine, New England Journal of Medicine 383(27) (2020) 2603-2615.

[22] S. Uchida, C.Y.J. Lau, M. Oba, K. Miyata, Polyplex designs for improving the stability and safety of RNA therapeutics, Advanced Drug Delivery Reviews 199 (2023) 114972.

[23] H. Bayraktutan, R. Kopiasz, A. ElSherbeny, M.M. Espuga, N. Gumus, U.C. Oz, K. Polra, P.F. McKay, R.J. Shattock, P.O. Moran, Polysarcosine functionalised cationic polyesters efficiently deliver self-amplifying mRNA, Polymer Chemistry (2024).

[24] K. Amin, N. Ashraf, L. Mao, C.F. Faul, Z. Wei, Conjugated microporous polymers for energy storage: Recent progress and challenges, Nano Energy 85 (2021) 105958.

[25] S. Uchida, K. Itaka, Q. Chen, K. Osada, T. Ishii, M.-A. Shibata, M. Harada-Shiba, K. Kataoka, PEGylated Polyplex With Optimized PEG Shielding Enhances Gene Introduction in Lungs by Minimizing Inflammatory Responses, Molecular Therapy 20(6) (2012) 1196-1203.

[26] C. Hald Albertsen, J.A. Kulkarni, D. Witzigmann, M. Lind, K. Petersson, J.B. Simonsen, The role of lipid components in lipid nanoparticles for vaccines and gene therapy, Advanced Drug Delivery Reviews 188 (2022) 114416.

[27] S. Tahtinen, A.-J. Tong, P. Himmels, J. Oh, A. Paler-Martinez, L. Kim, S. Wichner, Y. Oei, M.J. McCarron, E.C. Freund, Z.A. Amir, C.C. de la Cruz, B. Haley, C. Blanchette, J.M. Schartner, W. Ye, M. Yadav, U. Sahin, L. Delamarre, I. Mellman, IL-1 and IL-1ra are key regulators of the inflammatory response to RNA vaccines, Nature Immunology 23(4) (2022) 532-542.

[28] C. Li, A. Lee, L. Grigoryan, P.S. Arunachalam, M.K.D. Scott, M. Trisal, F. Wimmers, M. Sanyal, P.A. Weidenbacher, Y. Feng, J.Z. Adamska, E. Valore, Y. Wang, R. Verma, N. Reis, D. Dunham, R. O'Hara, H. Park, W. Luo, A.D. Gitlin, P. Kim, P. Khatri, K.C. Nadeau, B. Pulendran, Mechanisms of innate and adaptive immunity to the Pfizer-BioNTech BNT162b2 vaccine, Nature Immunology 23(4) (2022) 543-555.

[29] V. Brentville, M. Vankemmelbeke, R. Metheringham, P. Symonds, K. Cook, R. Urbanowicz, T. Tsoleridis, C. Coleman, K. Chang, A. Skinner, SARS-CoV-2 spike RBD and nucleocapsid encoding DNA vaccine elicits T cell and neutralising antibody responses that cross react with variants, bioRxiv (2021) 2021.06. 18.448932.

[30] P. Bankhead, M.B. Loughrey, J.A. Fernández, Y. Dombrowski, D.G. McArt, P.D. Dunne, S. McQuaid, R.T. Gray, L.J. Murray, H.G. Coleman, QuPath: Open source software for digital pathology image analysis, Scientific reports 7(1) (2017) 1-7.

[31] K. Guk, H. Lim, B. Kim, M. Hong, G. Khang, D. Lee, Acid-cleavable ketal containing poly (β-amino ester) for enhanced siRNA delivery, International journal of pharmaceutics 453(2) (2013) 541-550.

[32] J.C. Sunshine, D.Y. Peng, J.J. Green, Uptake and transfection with polymeric nanoparticles are dependent on polymer end-group structure, but largely independent of nanoparticle physical and chemical properties, Molecular pharmaceutics 9(11) (2012) 3375-3383.

[33] J. Kim, S.K. Mondal, S.Y. Tzeng, Y. Rui, R. Al-Kharboosh, K.K. Kozielski, A.G. Bhargav, C.A. Garcia, A. Quiñones-Hinojosa, J.J. Green, Poly(ethylene glycol)–Poly(beta-amino ester)-Based Nanoparticles for Suicide Gene Therapy Enhance Brain Penetration and Extend Survival in a Preclinical Human Glioblastoma Orthotopic Xenograft Model, ACS Biomaterials Science & Engineering 6(5) (2020) 2943-2955.

[34] M.W. Konstan, P.B. Davis, J.S. Wagener, K.A. Hilliard, R.C. Stern, L.J. Milgram, T.H. Kowalczyk, S.L. Hyatt, T.L. Fink, C.R. Gedeon, Compacted DNA nanoparticles administered to the nasal mucosa of cystic fibrosis subjects are safe and demonstrate partial to complete cystic fibrosis transmembrane regulator reconstitution, Human gene therapy 15(12) (2004) 1255-1269.

[35] J. Niu, D.J. Lunn, A. Pusuluri, J.I. Yoo, M.A. O'Malley, S. Mitragotri, H.T. Soh, C.J. Hawker, Engineering live cell surfaces with functional polymers via cytocompatible controlled radical polymerization, Nature Chemistry 9(6) (2017) 537-545.

[36] P. Gurnani, A.M. Lunn, S. Perrier, Synthesis of mannosylated and PEGylated nanoparticles via RAFT emulsion polymerisation, and investigation of particle-lectin aggregation using turbidimetric and DLS techniques, Polymer 106 (2016) 229-237.

[37] Y.-Z. Chen, X.-L. Yao, Y. Tabata, S. Nakagawa, J.-Q. Gao, Gene carriers and transfection systems used in the recombination of dendritic cells for effective cancer immunotherapy, Journal of Immunology Research 2010 (2010).

[38] C.H. Jones, M. Chen, A. Ravikrishnan, R. Reddinger, G. Zhang, A.P. Hakansson, B.A. Pfeifer, Mannosylated poly (beta-amino esters) for targeted antigen presenting cell immune modulation, Biomaterials 37 (2015) 333-344.

[39] B. Briard, D.E. Place, T.-D. Kanneganti, DNA Sensing in the Innate Immune Response, Physiology 35(2) (2020) 112-124.

[40] P.L. Ma, M.D. Buschmann, F.M. Winnik, Complete physicochemical characterization of DNA/chitosan complexes by multiple detection using asymmetrical flow field-flow fractionation, Analytical chemistry 82(23) (2010) 9636-9643.

[41] H. Jeong, J. Hwang, H. Lee, P.T. Hammond, J. Choi, J. Hong, In vitro blood cell viability profiling of polymers used in molecular assembly, Scientific reports 7(1) (2017) 1-13.

[42] Y. Phanse, A.E. Ramer-Tait, S.L. Friend, B. Carrillo-Conde, P. Lueth, C.J. Oster, G.J. Phillips, B. Narasimhan, M.J. Wannemuehler, B.H. Bellaire, Analyzing cellular internalization of nanoparticles and bacteria by multi-spectral imaging flow cytometry, JoVE (Journal of Visualized Experiments) (64) (2012) e3884.

[43] V.A. Brentville, M. Vankemmelbeke, R. Metheringham, P. Symonds, K. Cook, R. Urbanowicz, T. Tsoleridis, C. Coleman, K. Chang, A. Skinner, A novel bivalent DNA vaccine encoding both spike protein receptor-binding domain and nucleocapsid protein of SARS-CoV-2 to elicit T cell and neutralising antibody responses that cross react with variants, bioRxiv (2021) 2021.06. 18.448932.

[44] F.F. Fang, As the virus evolves, so too must we: a drug developer's perspective, Virology Journal 19(1) (2022) 1-5.

[45] C.G. Zamboni, K.L. Kozielski, H.J. Vaughan, M.M. Nakata, J. Kim, L.J. Higgins, M.G. Pomper, J.J. Green, Polymeric nanoparticles as cancer-specific DNA delivery vectors to human hepatocellular carcinoma, Journal of Controlled Release 263 (2017) 18-28.

[46] E. Ben-Akiva, J. Karlsson, S. Hemmati, H. Yu, S.Y. Tzeng, D.M. Pardoll, J.J. Green, Biodegradable lipophilic polymeric mRNA nanoparticles for ligand-free targeting of splenic dendritic cells for cancer vaccination, Proceedings of the National Academy of Sciences 120(26) (2023) e2301606120.

[47] C. Efe, A.V. Kulkarni, B. Terziroli Beretta-Piccoli, B. Magro, A. Stättermayer, M. Cengiz, D. Clayton-Chubb, C. Lammert, C. Bernsmeier, Ö. Gül, Liver injury after SARS-CoV-2 vaccination: Features of immune-mediated hepatitis, role of corticosteroid therapy and outcome, Hepatology 76(6) (2022) 1576-1586.

[48] D.G. Anderson, A. Akinc, N. Hossain, R. Langer, Structure/property studies of polymeric gene delivery using a library of poly(β-amino esters), Molecular Therapy 11(3) (2005) 426-434.

[49] A.M. Rokstad, O.-L. Brekke, B. Steinkjer, L. Ryan, G. Kolláriková, B.L. Strand, G. Skjåk-Bræk, J.D. Lambris, I. Lacík, T.E. Mollnes, T. Espevik, The induction of cytokines by polycation containing microspheres by a complement dependent mechanism, Biomaterials 34(3) (2013) 621-630.

[50] A.K. Blakney, P.F. McKay, C.R. Bouton, K. Hu, K. Samnuan, R.J. Shattock, Innate Inhibiting Proteins Enhance Expression and Immunogenicity of Self-Amplifying RNA, Molecular Therapy 29(3) (2021) 1174-1185.

[51] S. Mishra, P. Webster, M.E. Davis, PEGylation significantly affects cellular uptake and intracellular trafficking of non-viral gene delivery particles, European Journal of Cell Biology 83(3) (2004) 97-111.

Supporting Information

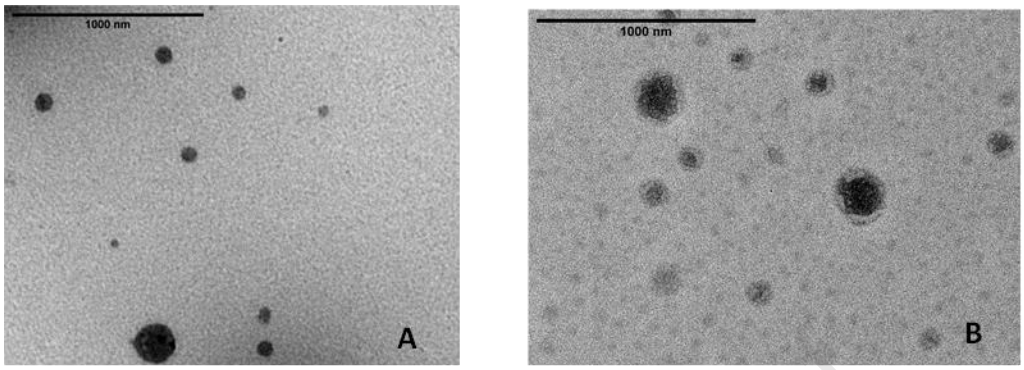

Figure S1: Representative transmission electron micrograph of *(A)* OH-(pBDD-5AP)-OH polyplexes and *(B)* Mix polyplexes. Scale bars correspond to 1000 nm.

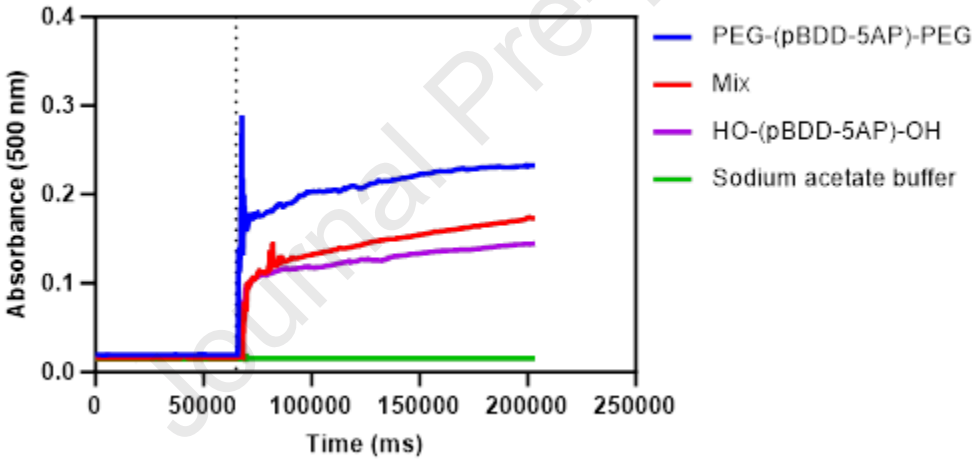

Figure S2: Absorbance-time curves of tannic acid-PEG binding assay measured on a UV-VIS spectrometer at 500 nm over 2 minutes with PEG-(pBDD-5AP)-PEG, OH-(pBDD-5AP)-OH and mix nanoparticles and sodium acetate buffer. Dotted line refers the time (65000 ms) that tannic acid was added to sodium acetate buffer and the nanoparticle suspensions.

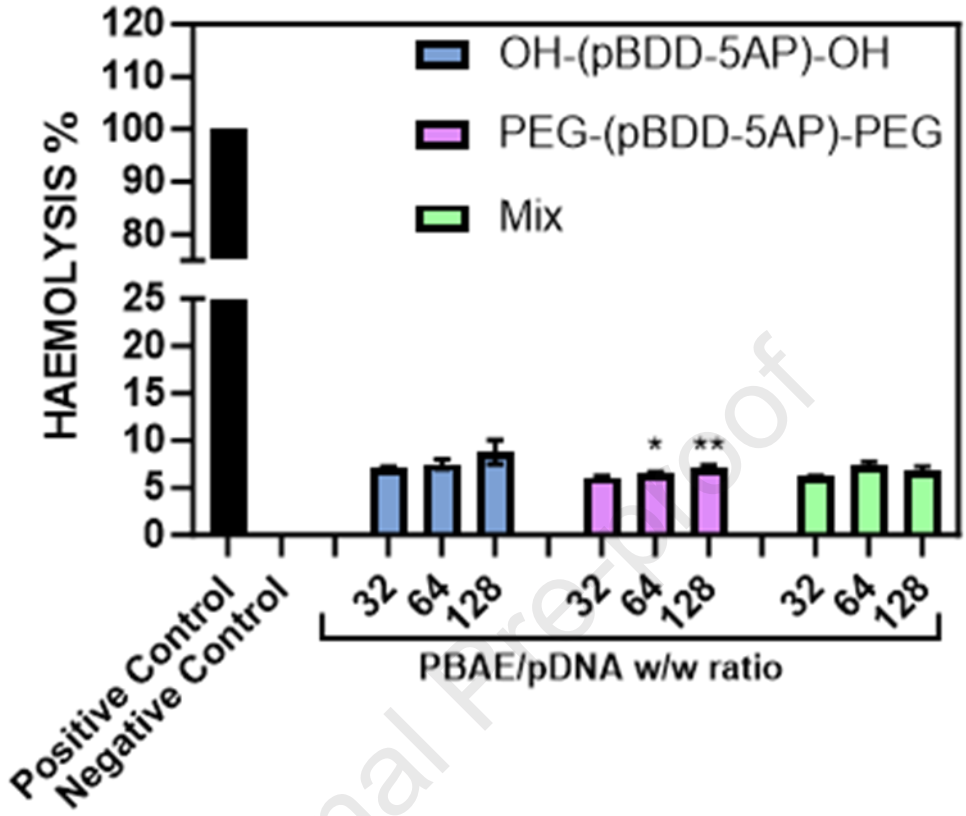

Figure S3: Hemolytic activity of OH-(pBDD-5AP)-OH, PEG-(pBDD-5AP)-PEG and 'mix' (a 1:1 w/w mixture of OH-(pBDD-5AP)-OH, PEG-(pBDD-5AP)-PEG) polyplexes at a PBAE/pDNA w/w ratio of 32, 64 and 128, measured after 2 h of incubation with human erythrocytes. Bars represented as the mean ± SD for n = 3. *$p < 0.5$ and **$p < 0.01$ (compared to non-PEGylated nanoparticles).

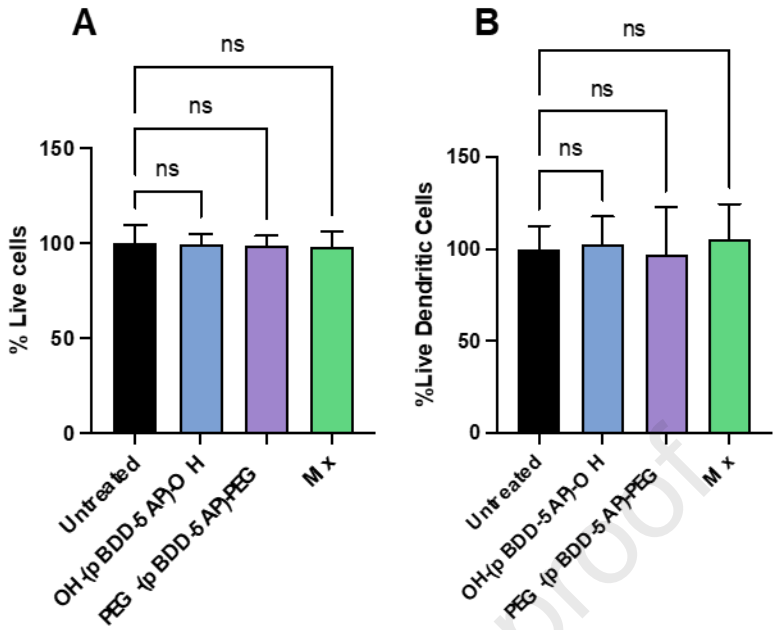

Figure S4: Live/Dead assay to determine effect of PBAE polyplexes at w/w 64 on BMDC cultures (N=3) determined using flow cytometry. (*A*) Live/Dead assay of total BM culture and (*B*) % of live MHC II + CD11c+ cells.

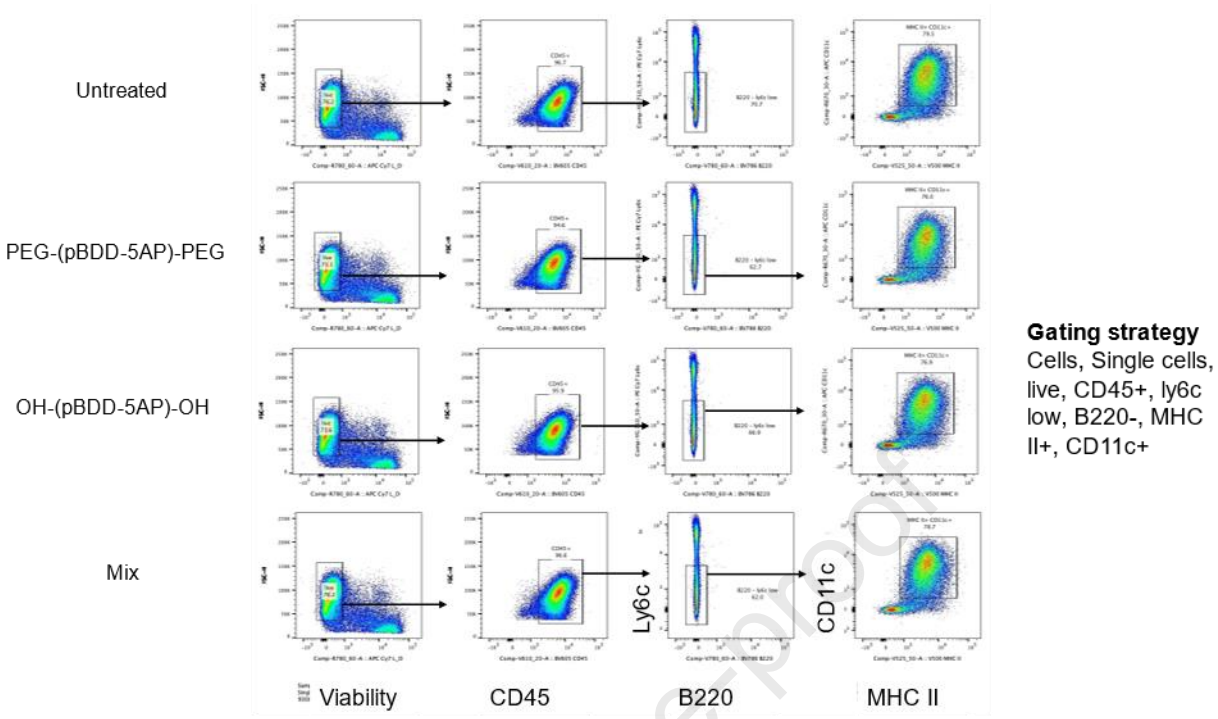

Figure S5 Gating strategy for flow cytometry analysis of % live cells and % live DCs.

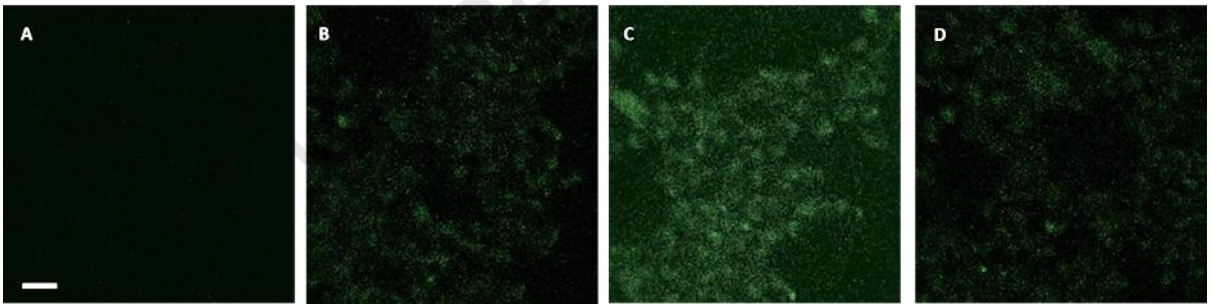

Figure S6: Live cell confocal microscopy original images of HEK293T cells 4 h post-transfection with an eGFP encoding pDNA formulated with *(A)* Nontreated *(B)* OH-(pBDD-5AP)-OH, *(C)* PEG-(pBDD-5AP)-PEG or *(D)* a 1:1 w/w mixture of OH-(pBDD-5AP)-OH and PEG-(pBDD-5AP)-PEG termed 'mix' at a PBAE/pDNA w/w ratio of 64. Scale bar corresponds to 20 µm (x40).

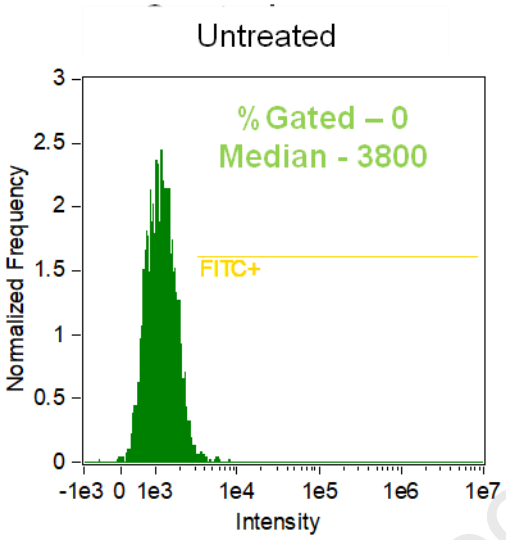

Figure S7: Imaging cytometry. Fluorescence intensity histogram of untreated group for DC2.4 cells. Data were analysed using IDEAS software.

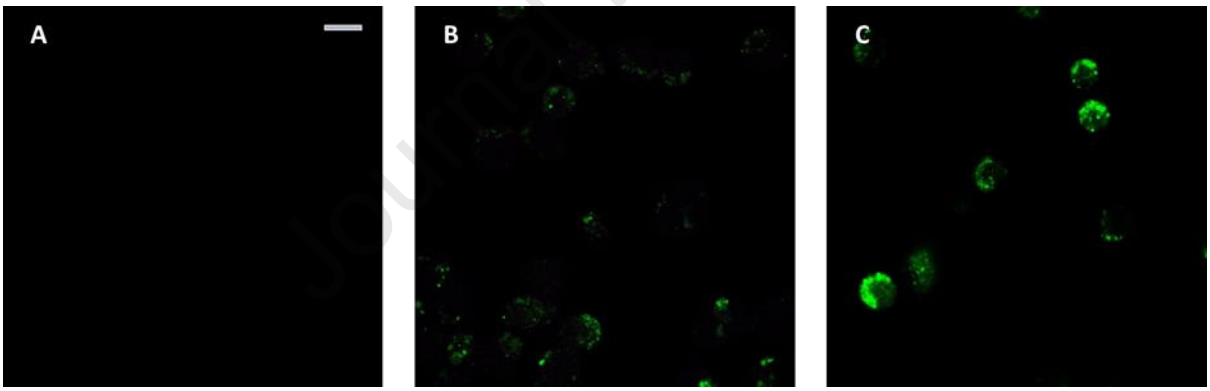

Figure S8: Live cell confocal microscopy original images of DC2.4 cells treated pDNA polyplexes derived from FITC-labelled PEG-(pBDD-5AP)-PEG at a PBAE/pDNA w/w ratio of 64 *(A)* Nontreated *(B)* after 1 h and *(C)* after 4 h at 100 ng/well (500 ng/mL) pDNA. Scale bar 10 µm (40x).

Image	Pearson's Correlation Coefficient
1	0.37
2	0.29
3	0.42
4	0.36
5	0.46

Table S1: Co-localisation with the acidic lysosomes with image analysis indicating Pearson's Correlation Coefficient between FITC labelled polyplexes and Lysotracker™ stained lysosomes were around 0.38.

Declaration of interests

☐ The authors declare that they have no known competing financial interests or personal relationships that could have appeared to influence the work reported in this paper.

☒ The authors declare the following financial interests/personal relationships which may be considered as potential competing interests:

Cameron Alexander. Pratik Gurnani reports financial support was provided by Wellcome Trust. Cameron Alexander reports financial support was provided by The Royal Society. Hulya Bayraktutan reports financial support was provided by Turkish Ministry of National Education. Peter Symonds, A Brentville, Lindy Durrant reports financial support was provided by Scancell Ltd. Peter Symonds, Victoria A Brentville, Lindy Durrant reports a relationship with Scancell Ltd that includes: employment and equity or stocks. None If there are other authors, they declare that they have no known competing financial interests or personal relationships that could have appeared to influence the work reported in this paper.